

Balancing Understanding and Generation in Discrete Diffusion Models

Yue Liu¹ Yuzhong Zhao¹ Zheyong Xie² Qixiang Ye¹ Jianbin Jiao¹ Yao Hu² Shaosheng Cao² Yunfan Liu¹

Abstract

In discrete generative modeling, two dominant paradigms demonstrate divergent capabilities: Masked Diffusion Language Models (MDLM) excel at semantic understanding and zero-shot generalization, whereas Uniform-noise Diffusion Language Models (UDLM) achieve strong few-step generation quality, yet neither attains balanced performance across both dimensions. To address this, we propose XDLM, which bridges the two paradigms via a stationary noise kernel. XDLM offers two key contributions: (1) it provides a principled theoretical unification of MDLM and UDLM, recovering each paradigm as a special case; and (2) an alleviated memory bottleneck enabled by an algebraic simplification of the posterior probabilities. Experiments demonstrate that XDLM advances the Pareto frontier between understanding capability and generation quality. Quantitatively, XDLM surpasses UDLM by 5.4 points on zero-shot text benchmarks and outperforms MDLM in few-step image generation (FID 54.1 vs. 80.8). When scaled to tune an 8B-parameter large language model, XDLM achieves 15.0 MBPP in just 32 steps, effectively doubling the baseline performance. Finally, analysis of training dynamics reveals XDLM’s superior potential for long-term scaling. Code is available at this http URL.

1. Introduction

Diffusion models have achieved remarkable success in continuous domains, particularly in image and audio generation (Ho et al., 2020; Dhariwal & Nichol, 2021; Rombach et al., 2022; Kong et al., 2020). Inspired by this potential, Discrete Denoising Diffusion Probabilistic Model (D3PM) has emerged as a promising paradigm shift to the discrete state space (Austin et al., 2021). Notably, these Discrete

Diffusion Models (DDMs) are now demonstrating strong performance in language modeling, a field long dominated by auto-regressive (AR) architectures.

Within this landscape, DDM studies have diverged into two distinct branches: Masked Diffusion Language Models (MDLMs) (Sahoo et al., 2024) and Uniform-noise Diffusion Language Models (UDLMs) (Schiff et al., 2024). While MDLMs achieve superior performance in likelihood modeling and zero-shot generalization, they often struggle to generate coherent, contextually consistent outputs with limited inference steps. Conversely, UDLMs excel at low-step generation but frequently lag behind MDLMs when the number of inference steps increases. Despite their individual merits, neither achieves balanced performance across these dimensions.

This imbalance carries significant practical implications. In domains like image synthesis, the required inference steps are typically far fewer than the total number of patches. In these few-step regimes, UDLM (and its hidden Gaussian counterparts (Schiff et al., 2024; Sahoo et al., 2025)) consistently outperforms the masked paradigm. Concretely, our experiments demonstrate that UDLM outperforms MDLM by 17.6% when generating ImageNet-1K images in an 8-step regime. Consequently, balancing the robust few-step generation of UDLMs with the superior semantic understanding of MDLMs remains a critical open challenge.

To this end, we propose miXed Diffusion Language Modeling (XDLM), a balanced theoretical formulation that establishes a rigorous bridge between uniform and masked noise distributions. Unlike GIDD (von Rütte et al., 2025), which relies on a computationally expensive time-inhomogeneous process where noise characteristics shift at every timestep, XDLM enforces a stationary noise kernel where incremental noise structurally matches the marginal noise, as shown in Fig. 1 (left). This consistency allows our training objective to be efficiently factorized into static constants and dynamic schedules, avoiding the complex re-computation of noise distributions required by GIDD. In addition, we prove that MDLM and UDLM are limiting cases of our formulation. Furthermore, XDLM enables a memory-efficient implementation by algebraically simplifying posterior calculations, allowing XDLM to scale to large vocabulary sizes without prohibitive computational costs.

¹UCAS ²Xiaohongshu Inc.. Correspondence to: Yunfan Liu <liyunfan@ucas.ac.cn>, Shaosheng Cao <caosheng@xiaohongshu.com>.

Stationary Noise Kernel

$$K = \begin{bmatrix} u & u & \cdots & u+m \\ u & u & \cdots & u+m \\ \vdots & \vdots & \ddots & \vdots \\ u & u & \cdots & u+m \end{bmatrix} \begin{matrix} \text{[NORMAL]} \\ \text{[MASK]} \\ \text{[NORMAL]} \\ \text{[MASK]} \end{matrix}$$

- $u \in \text{UDLM}$: Probability of transitioning to a random token (Uniform Noise).
- $m \in \text{MDLM}$: Probability of transitioning to the Mask state (Absorbing Noise).

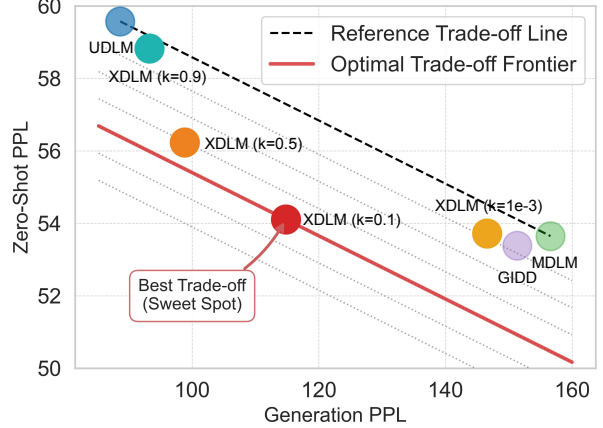


Figure 1. Left: XDLM combines the noise kernel of UDLM (u) and MDLM (m) to achieve a favorable trade-off between the two methods. [NORMAL] denotes normal tokens, while [MASK] represents the mask token. Right: The trade-off between understanding capability (zero-shot perplexity; lower is better) and generation capability (generation perplexity in 32 sampling steps; lower is better). The proposed XDLM with a mixing ratio of $k = 0.1$ achieves the optimal balance, labeled as the ‘Sweet Spot’.

Experimental results demonstrate that XDLM consistently achieves superior performance across diverse modalities, validating the efficacy of our balanced discrete diffusion approach. As illustrated in Fig. 1 (right), XDLM advances the Pareto frontier between understanding capability and generative quality. Notably, as the interpolation parameters shift toward their extremes, XDLM matches the performance of UDLM and MDLM respectively, confirming the model’s theoretical foundation. Concretely, in zero-shot language benchmarks, XDLM surpasses UDLM by 5.4 points in averaged metrics and trails MDLM by only 0.45. In conditional image generation, XDLM excels in both efficiency and quality: it significantly outperforms MDLM in few-step generation (reducing FID from 80.8 to 54.1 at 4 steps) and ranks first at 16 steps, surpassing UDLM by 0.4 points. Furthermore, large-scale continual pretraining on 8B-parameter LLMs (Nie et al., 2025) yields an MBPP score of 15.0 in only 32 sampling steps, improving upon the vanilla LLaDA baseline by over 120% (15.0 vs. 6.8). Finally, analysis of training dynamics reveals a distinct performance crossover: while masked baselines converge quickly but plateau early, XDLM sustains steady improvement throughout training, demonstrating superior long-term scaling.

2. Preliminary

Discrete Diffusion Models (DDMs) are latent generative models defined by two Markov processes: a *forward* process and a *reverse* process. Considering a single categorical variable \mathbf{x}_0 , represented as a one-hot vector in $\{0, 1\}^N$, where $N = |\mathcal{V}|$ denotes the vocabulary size. Let \mathbf{z}_t represent the latent state at time $t \in [0, 1]$, with $\mathbf{z}_0 := \mathbf{x}_0$. The forward process q progressively corrupts the data via transition kernels $q(\mathbf{z}_t \mid \mathbf{z}_s)$ for $s < t$, and the backward

process $p_\theta(\mathbf{z}_s \mid \mathbf{z}_t)$ parameterized by θ iteratively denoises the latent states to recover the clean data \mathbf{x}_0 .

Forward Process The forward transition probabilities are governed by row-stochastic matrix $\mathbf{Q}_{t|s} \in \mathbb{R}^{N \times N}$:

$$q(\mathbf{z}_t \mid \mathbf{z}_s) = \text{Cat}(\mathbf{z}_t; \mathbf{Q}_{t|s}^\top \mathbf{z}_s), \quad (1)$$

where \mathbf{z}_t and \mathbf{z}_s are one-hot vectors due to the discreteness of the latent states, and $\text{Cat}(\mathbf{x}; \mathbf{p})$ is a categorical distribution. Common structural choices for $\mathbf{Q}_{t|s}$ include uniform transitions (UDLM (Schiff et al., 2024)) and absorbing-state transitions (MDLM (Sahoo et al., 2024)).

Reverse Process Using Bayes’ rule and the Markov property, the posterior probability of \mathbf{z}_s given \mathbf{z}_t and \mathbf{x}_0 can be expressed as (Austin et al., 2021):

$$q(\mathbf{z}_s \mid \mathbf{z}_t, \mathbf{x}_0) = \frac{(\mathbf{Q}_{t|s} \mathbf{z}_t) \odot (\mathbf{Q}_{s|0}^\top \mathbf{x}_0)}{\mathbf{z}_t^\top \mathbf{Q}_{t|0}^\top \mathbf{x}_0}. \quad (2)$$

In literature, this reverse transition is approximated using the \mathbf{x}_0 -parameterization (Austin et al., 2021; Sahoo et al., 2024; Schiff et al., 2024), where a neural network f_θ is adopted to predict the distribution of clean data $\tilde{\mathbf{x}}_0 = f_\theta(\mathbf{z}_t)$. Thus, the parameterized reverse transition can be written as $p_\theta(\mathbf{z}_s \mid \mathbf{z}_t) = q(\mathbf{z}_s \mid \mathbf{z}_t, \tilde{\mathbf{x}}_0)$.

Training Objective The variational lower bound (VLB, ELBO) is optimized during training, which can be decomposed into three components: prior, diffusion, and reconstruction terms. Mathematically, define $s = (i - 1)/T$ and

$t = i/T$, the objective \mathcal{L}_{vb} can be formulated as:

$$\begin{aligned} \mathcal{L}_{\text{vb}} = & \mathbb{E}_{q(\mathbf{x}_0)} \left[\underbrace{D_{\text{KL}}(q(\mathbf{z}_1 \mid \mathbf{x}_0) \parallel p(\mathbf{z}_1))}_{\mathcal{L}_{\text{prior}}} \right. \\ & + \sum_{i=2}^T \underbrace{\mathbb{E}_{q(\mathbf{z}_t \mid \mathbf{x}_0)} [D_{\text{KL}}(q(\mathbf{z}_s \mid \mathbf{z}_t, \mathbf{x}_0) \parallel p_{\theta}(\mathbf{z}_s \mid \mathbf{z}_t))] }_{\mathcal{L}_{\text{diffusion}}} \\ & \left. - \underbrace{\mathbb{E}_{q(\mathbf{z}_{1/T} \mid \mathbf{x}_0)} [\log p_{\theta}(\mathbf{x}_0 \mid \mathbf{z}_{1/T})]}_{\mathcal{L}_{\text{recons}}} \right]. \end{aligned} \quad (3)$$

In the continuous time limit ($T \rightarrow \infty$), the prior and reconstruction terms reduce to 0, simplifying the objective to the diffusion term (Schiff et al., 2024):

$$\mathcal{L}_{\text{vb}} = \mathbb{E}_{t \sim \mathcal{U}(0,1)} [TD_{\text{KL}}(q(\mathbf{z}_s \mid \mathbf{z}_t, \mathbf{x}_0) \parallel p_{\theta}(\mathbf{z}_s \mid \mathbf{z}_t))]. \quad (4)$$

3. miXed Diffusion Language Modeling via Stationary Noise Kernels

This section details the proposed miXed Diffusion Language Modeling (XDLM) framework. It begins by introducing the forward process with a stationary noise kernel in Sec. 3.1, and then derives a scalar formulation for efficient sampling and training in Sec. 3.2. Finally, Sec. 3.3 establishes that UDLM and MDLM can be viewed as limiting cases of XDLM under particular settings of the hybrid parameter.

3.1. The Forward Process with Stationary Kernels

The forward diffusion process of DDMs from time s to t is governed by a transition matrix $\mathbf{Q}_{t|s}$, defined as a convex combination of the signal-preserving identity matrix \mathbf{I} and a stationary noise kernel \mathbf{K} :

$$\mathbf{Q}_{t|s} = \alpha_{t|s} \mathbf{I} + \beta_{t|s} \mathbf{K}, \quad (5)$$

where $\alpha_{t|s}, \beta_{t|s} \in [0, 1]$ represent a scalar schedule satisfying $\alpha_{t|s} + \beta_{t|s} = 1$.

A critical design choice in our method is the stationarity of \mathbf{K} . Unlike GIDD (von Rütte et al., 2025), which utilizes time-dependent mixing distributions that inherently couple the noise structure with the diffusion timeline, we enforce \mathbf{K} to remain invariant across all time steps. This stationarity decouples the noise characteristics from the scheduling dynamics, ensuring that the diffusion process follows a geometrically consistent trajectory toward a fixed target distribution, which aligns with the optimal transport path proposed in the Flow Matching (Lipman et al., 2022).

Under this constraint, the noise kernel \mathbf{K} must map every input state toward a target noise distribution π , regardless of the starting state. This requirement is formalized next.

Lemma 3.1 (Construction of Mixing Kernel). *Let $\pi \in \mathcal{R}^N$ be a stationary target distribution defined as a mixture of the uniform distribution \mathbf{u} and point-masses on special tokens $i \in \mathcal{S}$. If the noise kernel \mathbf{K} satisfies the property of instantaneous mixing (i.e., convergence to π in a single step), it admits the decomposition:*

$$\mathbf{K} = \frac{k}{N} \mathbf{J} + \sum_{i \in \mathcal{S}} \mu_i \mathbf{M}_i, \quad (6)$$

where \mathbf{J} is the all-ones matrix, \mathbf{M}_i is the absorbing matrix for state i , and the weights satisfy $k + \sum \mu_i = 1$.

We specialize Lemma 3.1 (derivation in Appendix A) to a standard MDLM setting with a single mask token, represented by the one-hot vector \mathbf{m} . By letting k and μ denote the weights of the uniform and masking components, respectively, the resulting noise kernel matrix naturally interpolates between the uniform noise and the mask state:

$$\mathbf{K} = \frac{k}{N} \mathbf{J} + \mu \mathbf{M}. \quad (7)$$

Fig. 1 illustrates the transition dynamics within the noise kernel K , driven by uniform noise and absorbing noise (mask state), labeled \mathbf{u} and \mathbf{m} , respectively.

3.2. Efficient Sampling and Training via Scalar Formulation

By substituting the definitions of the noise kernel \mathbf{K} (Eq. 6) and transition matrix $\mathbf{Q}_{t|s}$ (Eq. 5) into Eq. 2 and Eq. 4, the detailed formulations for the posterior $q(\mathbf{z}_s \mid \mathbf{z}_t, \mathbf{x})$ and KL divergence can be readily obtained. However, direct evaluation of these expressions via matrix operations is prohibitively expensive in terms of both memory and computation, particularly for large vocabularies. In this section, we derive that the posterior and KL divergence can be reformulated into an equivalent scalar form with Lemma 3.3 and Lemma 3.4. By further incorporating the asymptotic limit behavior defined in Lemma 3.5, we establish a tractable and numerically stable training objective that bypasses the expensive explicit computation of large vocabulary size.

Concretely, let \mathbf{e} denote an arbitrary one-hot basis vector, the posterior probability of transitioning to state \mathbf{e} can thus be written as

$$\begin{aligned} q(\mathbf{z}_s = \mathbf{e} \mid \mathbf{z}_t, \mathbf{x}) &= \mathbf{e}^\top \frac{(\alpha_{t|s} \mathbf{z}_t + \beta_{t|s} K \mathbf{z}_t) \odot (\alpha_s \mathbf{x} + \beta_s K^\top \mathbf{x})}{\mathbf{z}_t^\top (\alpha_t \mathbf{x} + \beta_t K^\top \mathbf{x})}, \end{aligned} \quad (8)$$

We observe that Eq. 8 can be reformulated into an equivalent scalar form by defining a set of helper functions, which can significantly reduce the computational complexity for both the posterior and the KL divergence.

Definition 3.2 (Scalar Primitives). Let $p_{\mathbf{x}, \mathbf{e}} := \mathbf{e}^\top \mathbf{x}$ represent the probability mass of distribution \mathbf{x} at token \mathbf{e} . We define the noise rate function $r(\mathbf{e})$ and the forward diffusion map $f_t(\mathbf{x}, \mathbf{e})$ as:

$$r(\mathbf{e}) = \frac{k}{N} + \mu \delta_{\mathbf{e}, \mathbf{m}} \quad (9)$$

$$f_t(\mathbf{x}, \mathbf{e}) = \alpha_t p_{\mathbf{x}, \mathbf{e}} + \beta_t r(\mathbf{e}) \quad (10)$$

These helper functions yield the following efficient expressions for the posterior and KL divergence, with full derivations deferred to Appendix B.

Lemma 3.3 (Scalar Posterior). *The posterior probability of transitioning to state \mathbf{e} can be formulated as:*

$$q(\mathbf{z}_s = \mathbf{e} \mid \mathbf{z}_t, \mathbf{x}) = \frac{f_s(\mathbf{x}, \mathbf{e}) f_{t|s}(\mathbf{e}, \mathbf{z}_t)}{f_t(\mathbf{x}, \mathbf{z}_t)}. \quad (11)$$

The model's reverse transition p_θ follows the same form by substituting \mathbf{x} with the predicted distribution $\tilde{\mathbf{x}}_0$.

Lemma 3.4 (Scalar KL Divergence). *The term $D_{KL}(q(\mathbf{z}_s \mid \mathbf{z}_t, \mathbf{x}) \parallel p_\theta(\mathbf{z}_s \mid \mathbf{z}_t))$ can be written as:*

$$D_{KL} = \frac{\beta_{t|s} \alpha_s r(\mathbf{z}_t)}{f_t(\mathbf{x}, \mathbf{z}_t)} h_t(\mathbf{x}, \mathbf{z}_t, \tilde{\mathbf{x}}_0), \quad (12)$$

where h_t is an auxiliary function collecting the logarithmic difference terms:

$$\begin{aligned} h_t(\mathbf{x}, \mathbf{z}_t, \tilde{\mathbf{x}}_0) &= \frac{f_s(\mathbf{x}, \mathbf{z}_t)}{r(\mathbf{z}_t)} \frac{\alpha_{t|s}}{\beta_{t|s} \alpha_s} \log \frac{f_s(\mathbf{x}, \mathbf{z}_t) f_t(\tilde{\mathbf{x}}_0, \mathbf{z}_t)}{f_t(\mathbf{x}, \mathbf{z}_t) f_s(\tilde{\mathbf{x}}_0, \mathbf{z}_t)} \\ &\quad - \frac{1}{\alpha_s} \log \frac{f_t(\mathbf{x}, \mathbf{z}_t)}{f_t(\tilde{\mathbf{x}}_0, \mathbf{z}_t)} + \log \frac{f_s(\mathbf{x}, \mathbf{x})}{f_s(\tilde{\mathbf{x}}_0, \mathbf{x})} \\ &\quad + \frac{k \beta_s}{N \alpha_s} \sum_{\mathbf{e} \in \mathcal{V}} \log \frac{f_s(\mathbf{x}, \mathbf{e})}{f_s(\tilde{\mathbf{x}}_0, \mathbf{e})}. \end{aligned} \quad (13)$$

As for the limiting case where $s \rightarrow t$, approximating continuous time, the auxiliary function h_t simplifies, thereby circumventing the numerical instability associated with the first logarithmic term in Eq. 13.

Lemma 3.5 (Limiting Case). *As $s \rightarrow t$, the function h_t converges to:*

$$\begin{aligned} h_t(\mathbf{x}, \mathbf{z}_t, \tilde{\mathbf{x}}_0) &\approx \frac{p_{\mathbf{x}, \mathbf{z}_t} - p_{\tilde{\mathbf{x}}_0, \mathbf{z}_t}}{f_t(\tilde{\mathbf{x}}_0, \mathbf{z}_t)} - \frac{1}{\alpha_t} \log \frac{f_t(\mathbf{x}, \mathbf{z}_t)}{f_t(\tilde{\mathbf{x}}_0, \mathbf{z}_t)} + \\ &\quad \log \frac{f_t(\mathbf{x}, \mathbf{x})}{f_t(\tilde{\mathbf{x}}_0, \mathbf{x})} + \frac{k \beta_t}{N \alpha_t} \sum_{\mathbf{e} \in \mathcal{V}} \log \frac{f_t(\mathbf{x}, \mathbf{e})}{f_t(\tilde{\mathbf{x}}_0, \mathbf{e})}. \end{aligned} \quad (14)$$

Consequently, by substituting the asymptotic behavior derived in Lemma 3.4 and 3.5 into the training objective defined in Eq. 4, we arrive at a tractable scalar formulation for the training loss:

$$\lim_{T \rightarrow \infty} \mathcal{L}_{\text{vb}} = \mathbb{E}_{t, \mathbf{x}_0, \mathbf{z}_t} \left[\frac{-\alpha'_t r(\mathbf{z}_t)}{f_t(\mathbf{x}, \mathbf{z}_t)} \cdot h_t(\mathbf{x}, \mathbf{z}_t, \tilde{\mathbf{x}}_0) \right]. \quad (15)$$

This substitution bypasses the expensive explicit computation of posterior distributions and their KL divergence, facilitating an efficient and stable implementation for XDLM training and sampling.

3.3. Relationship to MDLM and UDLM

The proposed XDLM generalizes existing DDM frameworks. Through the modulation of the uniform noise weight k (Eq. 7), and the consequent adjustment of the absorbing strength, XDLM reduces to UDLM and MDLM at the parameter's limits. The relationship between XDLM and these models is outlined in this section, with a detailed analysis deferred to Appendix C.

Connection with MDLM. Setting $k = 0$ (which implies $\mu = 1$) reduces the noise kernel to a pure masking operation. Thus, the posterior probability simplifies to:

$$\begin{aligned} p_\theta(\mathbf{z}_s = \mathbf{e} \mid \mathbf{z}_t) &= \delta_{\mathbf{z}_t, \mathbf{m}} \delta_{\mathbf{e}, \mathbf{m}} \frac{\beta_s}{\beta_t} + \delta_{\mathbf{z}_t, \mathbf{m}} \delta_{\mathbf{e} \neq \mathbf{m}} \frac{\beta_{t|s} \alpha_s p_{\theta, \mathbf{e}}}{\beta_t} + \delta_{\mathbf{z}_t \neq \mathbf{m}} \delta_{\mathbf{e}, \mathbf{z}_t} \\ &= \begin{cases} \frac{\beta_s}{\beta_t} \delta_{\mathbf{m}, \mathbf{z}_t}, & \mathbf{e} = \mathbf{m} \\ \frac{(\alpha_s - \alpha_t)}{1 - \alpha_t} p_{\theta, \mathbf{e}}, & \mathbf{z}_t = \mathbf{m}, \mathbf{e} \neq \mathbf{m} \\ \delta_{\mathbf{e}, \mathbf{z}_t}, & \mathbf{z}_t \neq \mathbf{m}, \mathbf{e} \neq \mathbf{m} \end{cases} \end{aligned} \quad (16)$$

Consequently, the KL divergence collapses to the standard cross-entropy loss on masked tokens, matching the MDLM objective (Sahoo et al., 2024):

$$\mathcal{L}_{\text{KL}} = -\frac{\beta_{t|s} \alpha_s}{\beta_t} \log p_\theta(\mathbf{x} \mid \mathbf{z}_t). \quad (17)$$

Connection with UDLM. Setting $k = 1$ (implying $\mu = 0$) yields the uniform noise kernel. In this limit, the posterior probability becomes:

$$\begin{aligned} p_\theta(\mathbf{z}_s = \mathbf{e} \mid \mathbf{z}_t) &= \frac{\delta_{\mathbf{e}, \mathbf{z}_t} (N \alpha_t p_{\theta, \mathbf{e}} + \beta_s \alpha_{t|s}) + (\alpha_s - \alpha_t) p_{\theta, \mathbf{e}} + \beta_s \beta_{t|s} / N}{N \alpha_t p_{\theta, \mathbf{z}_t} + \beta_t} \end{aligned} \quad (18)$$

Define $\bar{\mathbf{x}}_j = \mathbf{N} \mathbf{f}_t(\mathbf{x}, \mathbf{e}_j)$, $(\bar{\mathbf{x}}_\theta)_j = \mathbf{N} \mathbf{f}_t(\tilde{\mathbf{x}}_0, \mathbf{e}_j)$ and considering the limit $s \rightarrow t$, our derived KL divergence aligns exactly with the UDLM loss derived in (Schiff et al., 2024):

$$\text{KL} = \frac{-\beta_{t|s} \alpha_s}{N \alpha_t} \left(\frac{N}{(\bar{\mathbf{x}}_\theta)_i} - \frac{N}{\bar{\mathbf{x}}_i} - \sum_{j: s.t. (\mathbf{z}_t)_j = 0} \frac{\bar{\mathbf{x}}_j}{\bar{\mathbf{x}}_i} \log \frac{(\bar{\mathbf{x}}_\theta)_i \bar{\mathbf{x}}_j}{(\bar{\mathbf{x}}_\theta)_j \bar{\mathbf{x}}_i} \right) \quad (19)$$

where i is the index of the active state in \mathbf{z}_t .

Table 1. Validation PPL on the OWT dataset. XDLM achieves performance comparable to MDLM and outperforms UDLM under the same training steps.

Model	MDLM	GIDD	XDLM	UDLM
PPL	23.321	23.136	24.097	25.937

4. Experiment

The experimental setup is first introduced in Sec. 4.1, with additional details provided in Appendix F. Sec. 4.2 then reports the performance of XDLM on zero-shot likelihood, language generation quality, and image generation tasks, demonstrating its superiority over existing methods, with more results presented in Appendix G, H and I. In addition, to evaluate scalability to larger model sizes, XDLM is further extended to LLaDA-XDLM via continual pretraining on LLaDA, which achieves strong performance on standard benchmarks (More details in Appendix J). Finally, Sec. 4.3 presents analysis and visualizations across different tasks, showing that XDLM achieves a better balance between understanding and generation than other approaches (More results in Appendix K, L, D and E).

4.1. Experimental Setup

All experiments were conducted on a cluster of $8 \times$ H800 GPUs. We standardized key hyperparameters where applicable, utilizing the AdamW optimizer ($\beta_1 = 0.9$, $\beta_2 = 0.999$, weight decay 0), a mixing ratio of $k = 0.1$, a global batch size of 512, and an EMA rate of 0.9999.

4.2. Performance

Evaluation of Zero-Shot Likelihood. To assess the generalization capabilities of XDLM, we evaluate zero-shot perplexity (PPL) on seven external datasets after training on OpenWebText (OWT). Aligning with prior work (Sahoo et al., 2024; 2025), our evaluation suite includes the validation splits of AG News (Zhang et al., 2015), LAMBADA (Paperno et al., 2016), LM1B (Chelba et al., 2013), Penn Treebank (Marcus et al., 1993), Scientific Papers from ArXiv and PubMed (Cohan et al., 2018), and WikiText (Merity et al., 2016). The validation PPL is estimated via the negative Evidence Lower Bound (ELBO) with Monte Carlo sampling. To ensure a fair comparison, we adopt the identical sampling configuration in (Sahoo et al., 2024; 2025).

As shown in Tab. 1, XDLM achieves a PPL of 24.097 on the OWT validation set, comparable to MDLM and GIDD and significantly outperforming UDLM (25.937). This retention of in-domain capability extends to zero-shot benchmarks. As listed in Tab. 2, XDLM obtains an average PPL of 54.110 across seven datasets, performing similarly to MDLM (53.650) and GIDD (53.384) while UDLM clearly lags behind (59.574).

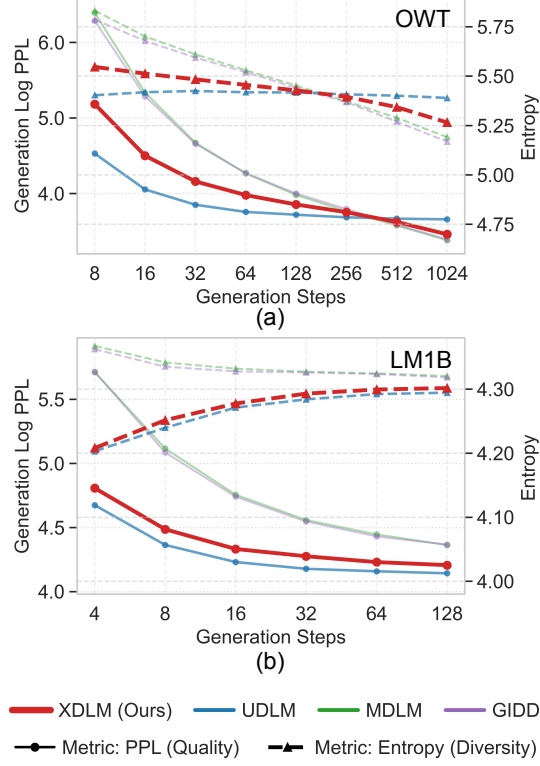


Figure 2. Language Generation Quality. Results on OWT (top) and LM1B (bottom) demonstrate that XDLM achieves a better balance across both few-step and multi-step regimes. For clarity, PPL and Generation Steps are reported in logarithmic scale.

Language Generation Quality. We evaluate performance using perplexity (quality) and token entropy (diversity) under *ancestral* sampling (Sahoo et al., 2024; Schiff et al., 2024; Sahoo et al., 2025). Fig. 2 shows that XDLM strikes a robust balance between masked and uniform diffusion paradigms. In few-step regimes (8–32 steps on OWT), XDLM benefits from uniform noise dynamics, achieving generation quality comparable to UDLMs and clearly surpassing purely masked models. In contrast, under multi-step regimes (512–1024 steps), masked noise becomes dominant, allowing XDLM to outperform UDLMs and reach MDLM-level performance. A similar trend is observed on LM1B, confirming the efficacy of XDLM in securing the efficiency of uniform noise while preserving the rigorous structure of masking. Comprehensive numerical results analyzing the impact of the mixing ratio k are provided in Appendix H.

Image Generation Performance. We evaluate domain generality via class-conditional generation on ImageNet-1K. Tab. 3 reports FID and IS scores without Classifier-Free Guidance (CFG). In few-step regimes, XDLM and UDLM consistently outperform mask-based baselines (*i.e.*, MDLM and GIDD). XDLM proves highly competitive with UDLM, achieving the lowest FID (25.77) at 16 steps, demonstrating its capacity for efficient, high-quality generation. When

Table 2. Zero-shot performance comparison across various benchmarks. XDLM maintains performance parity with MDLM and GIDD, significantly outperforming UDLM. Models were reimplemented under a unified setting using 8×H800 GPUs.

Dataset	AG News	LAMBADA	LM1B-GPT2	PTB	ArXiv	PubMed	WikiText	Average
MDLM	61.374	47.967	65.629	89.049	37.457	41.981	32.093	53.650
GIDD	60.607	47.811	65.898	86.911	39.019	42.634	30.809	53.384
XDLM	62.768	45.608	68.229	90.796	37.232	41.391	32.748	54.110
UDLM	69.402	51.272	75.572	95.986	42.671	47.181	34.933	59.574

Table 3. Performance comparison of image generation on ImageNet-1K with standard conditioning.

Model	FID ↓			IS ↑		
	step 4	step 8	step 16	step 4	step 8	step 16
MDLM	80.752	47.732	28.785	16.287	29.178	44.656
GIDD	86.842	54.933	35.403	14.559	24.297	35.698
XDLM	54.085	34.109	25.774	24.829	36.964	43.903
UDLM	49.861	30.144	26.242	27.049	38.832	41.801

Table 4. Performance comparison of image generation on ImageNet-1K with $\text{CFG scale} = 2.0$.

Model	FID ↓			IS ↑		
	step 4	step 8	step 16	step 4	step 8	step 16
MDLM	33.468	11.144	6.725	54.740	119.150	172.664
GIDD	41.000	15.151	7.076	44.084	95.789	148.148
XDLM	13.550	8.956	8.625	107.403	148.723	165.916
UDLM	14.055	9.718	8.980	97.859	123.582	132.099

evaluating with CFG (scale=2.0), as shown in Tab. 4, the pure mask-based MDLM achieves the lowest overall FID (6.73) at 16 steps, suggesting that masking excels given sufficient steps. However, by partially inheriting these absorbing noise properties, XDLM significantly outperforms UDLM in the few-step regime, achieving the best FID scores at 4 steps (13.55) and 8 steps (8.96). Extended analysis is provided in Appendix I.

Continual Pretraining of Large Language Models (LLMs). To validate XDLM as a scalable upgrade for state-of-the-art LLMs, we adapt LLaDA (Nie et al., 2025), a pretrained 8B-MDLM, into the XDLM formulation with a compute-efficient pretraining of 600 steps (termed LLaDA-XDLM). To rigorously isolate the source of improvement, we compare against two controls: LLaDA-MDLM (standard continual pretraining for the same duration) and LLaDA-XDLM-infer (LLaDA coupled with our sampling strategy).

Evaluations on OpenCompass (32 steps) show that LLaDA-XDLM consistently outperforms the original LLaDA and both controls on GSM8k, MATH, and BBH (Fig. 3 (a)). The impact is most visible in MBPP code generation, where LLaDA-XDLM doubles the performance of LLaDA (15.0 vs. 6.8) by minimizing non-compilable errors, thereby confirming enhanced structural coherence.

As for the control models, while LLaDA-MDLM suffers a

performance drop compared to the original LLaDA, likely due to a distribution shift between the tuning and pretraining corpora, LLaDA-XDLM achieves significant improvements under identical conditions. This confirms that the gains stem from the efficacy of the XDLM formulation rather than the additional 600 training steps alone. Furthermore, LLaDA-XDLM remarkably outperforms LLaDA-XDLM-infer, demonstrating that the improvement is intrinsic to the learned model rather than an artifact of sampling strategies.

4.3. Analysis

Performance Crossover in Training Dynamics. Analysis of the training dynamics reveals a ‘performance crossover’ phenomenon, where the relative efficacy of competing models shifts significantly as training progresses. This trend is particularly evident in the LM1B text generation task, as shown by the Generation PPL curves in Figure 4 (a). While GIDD and MDLM demonstrate advantages in the initial phase (<200k steps, pink region), they suffer from rapid saturation and are eventually outperformed by UDLM (yellow region). Leveraging the uniform nature inherited from UDLM, XDLM demonstrates substantial late-stage improvement, eventually matching or surpassing MDLM after 700k steps (green region). This trajectory is in sharp contrast to GIDD, which exhibits early saturation and only marginal PPL gains throughout the training process.

A different, yet similar in trends, dynamic emerges in image generation on ImageNet-1K, as shown in Fig. 4 (b). Here, XDLM demonstrates superior performance from the start, consistently achieving the lowest FID scores. While UDLM eventually converges with XDLM in the final training phase (> 500k steps), both models significantly outperform the MDLM and GIDD baselines throughout the process.

Impact of Mixing Ratio. The mixing ratio k acts as a pivotal control parameter, interpolating between two distinct paradigms: UDLM ($k \rightarrow 1$) and MDLM ($k \rightarrow 0$), characterized by their divergent capabilities in generation and understanding. As shown in Fig. 1 (right), these boundary cases establish a linear *Reference Trade-off Line* (dashed black line), representing a zero-sum scenario where gains in generation quality (lower Generation PPL) come at the cost of understanding capability (higher Zero-Shot PPL).

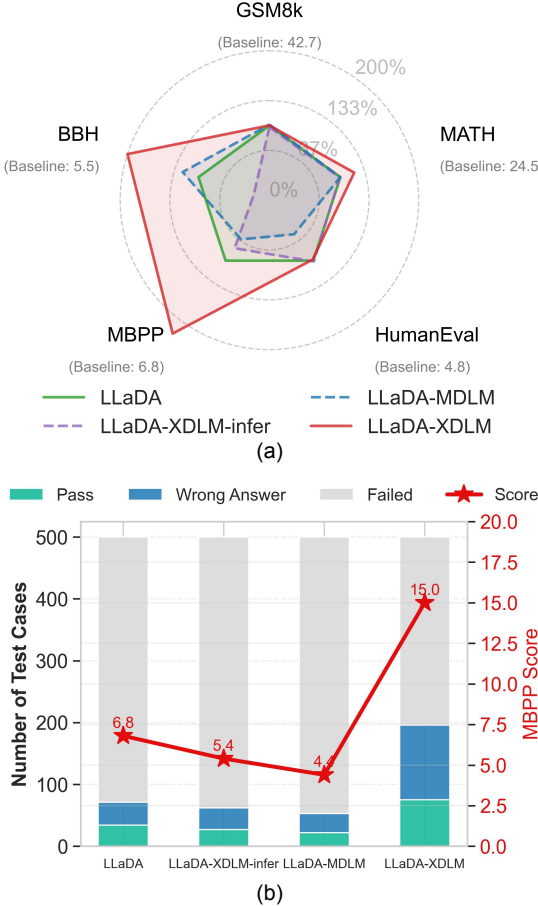


Figure 3. Evaluation of adapting LLaDA-8B to our XDLM formulation (LLaDA-XDLM): (a) LLaDA-XDLM consistently outperforms baselines across diverse benchmarks; (b) Improvements are particularly pronounced in code generation (MBPP), where the model substantially reduces generation failures.

However, the empirical behavior of XDLM reveals that the model does not merely traverse this linear path. Crucially, varying k shifts the model’s operating point along a continuous, smooth trajectory. This coherent evolution, as opposed to stochastic fluctuations or random walks, validates the architectural design, confirming that XDLM successfully synthesizes the mechanical properties of both UDLM and MDLM into a unified framework. Moreover, this trajectory bows inward to form a superior *Optimal Trade-off Frontier* (solid red line), demonstrating a synergistic effect where the mixed objective yields performance gains that exceed the sum of the parts. By navigating this frontier, we identify an empirical ‘sweet spot’ at $k = 0.1$. As shown by the red marker, this configuration effectively breaks the Pareto frontier of the baselines, achieving robust understanding capabilities without the severe degradation in generation performance typical of pure masked models.

Computational Efficiency of XDLM. We analyze the computational efficiency across inference, training, and sam-

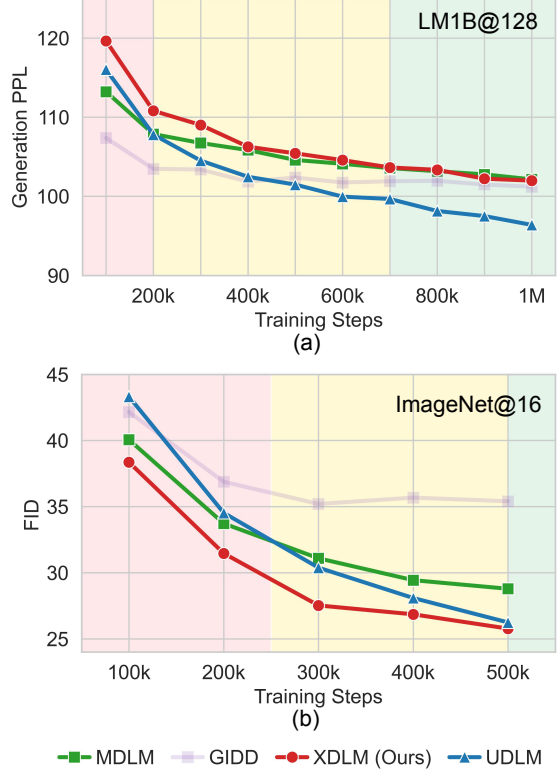


Figure 4. Training dynamics for (a) text and (b) image generation tasks. Colored regions indicate the dominant model during each phase, while transitions between colors mark points of performance crossover.

pling. While MDLM remains the fastest baseline due to its simple absorbing kernel, XDLM emerges as the most efficient model among those involving uniform noise. Benefiting from our scalar reformulated strategy, XDLM achieves a forward throughput of 396,398 tokens/s, nearly double GIDD’s 199,516 tokens/s, and a training throughput of 137,372 tokens/s. In generation tasks, XDLM maintains a sampling speed of 7,108 tokens/s, significantly surpassing UDLM (2,882 tokens/s). This efficiency extends to memory consumption, where XDLM requires only 31.4 GB compared to UDLM’s 59.7 GB and GIDD’s 40.9 GB. These results confirm that XDLM effectively mitigates large-vocabulary bottlenecks without compromising the expressivity of complex noise kernels. For more detailed results, please refer to Appendix K.

Inference Dynamics. To investigate the internal generation mechanism of XDLM, we closely inspect a single generation trajectory over a budget of $T = 32$ steps. The result shows that XDLM effectively leverages a hybrid noise process: it constructs semantic structure via absorbing noise ($[\text{MASK}] \rightarrow \text{Token}$) while refining content through uniform noise ($\text{Token} \rightarrow \text{Token}$). Crucially, XDLM distinguishes itself with a re-masking strategy (transforming tokens back to $[\text{MASK}]$). Unlike standard iterative models that exhibit

high sensitivity to initialization noise, this mechanism allows XDLM to actively reject low-probability tokens derived from uniform noise, effectively escaping local optima. For a detailed analysis, please refer to Appendices D and E.

5. Related work

Masked Diffusion Language Modeling. Building on the general and flexible discrete diffusion framework introduced by D3PM (Austin et al., 2021), absorbing-state-based corruptions (often using a special [MASK] token) have emerged as a popular paradigm for discrete diffusion in language, frequently referred to as Masked Diffusion Language Models (MDLMs). MDLM (Sahoo et al., 2024) and MD4 (Shi et al., 2024) extend this framework and derive a continuous-time variational objective for masked diffusion as a simple weighted integral of cross-entropy losses, yielding a streamlined and general training recipe for discrete language models. From a continuous-time perspective, CTMC (Campbell et al., 2022) formalizes the forward process via continuous-time Markov chains, while SEDD (Lou et al., 2023) learns density ratios directly, providing a discrete analogue of score matching. These advances have facilitated scaling masked diffusion LMs to larger model sizes and datasets, leading to large diffusion language models such as LLaDA (Nie et al., 2025) and Dream (Ye et al., 2025), as well as extensions to multimodal settings (You et al., 2025; Yang et al., 2025; Yu et al., 2025).

Uniform-noise Diffusion Language Modeling. The transition kernel of uniform-noise diffusion is a mixture of the identity and a uniform distribution over the vocabulary. This idea was introduced for discrete spaces in Argmax/Multinomial diffusion (Hoogeboom et al., 2021) and generalized by D3PM (Austin et al., 2021). Plaid (Gulrajani & Hashimoto, 2023) takes a notable step toward narrowing the likelihood gap between autoregressive models and diffusion-based language models. UDLM (Schiff et al., 2024) shows that, with appropriate guidance mechanisms, uniform-noise diffusion can yield stronger controllability. Duo (Sahoo et al., 2025) highlights a duality between Gaussian diffusion language models (e.g., Plaid) and uniform-noise diffusion, and proposes distilling a uniform-noise model from an auxiliary latent Gaussian model.

Mixed Language Modeling. D3PM (Austin et al., 2021) observes that BERT can be viewed as a one-step instance of mixed corruption with transition matrix. However, BERT is trained with a cross-entropy objective on the masked positions only, whereas diffusion-based approaches optimize objectives integrated over a noise schedule (or time), leading to different training dynamics and inductive biases.

Recent research has further bridged and generalized these paradigms. (Fathi et al., 2025) unify autoregressive and

diffusion models by assigning distinct noise schedules to individual token positions. Similarly, ReMDM (Wang et al., 2025) relaxes the strict absorbing constraint of the forward process, allowing [MASK] tokens to revert to their original states, thereby enabling plug-and-play editing capabilities.

Our most related work is GIDD (von Rütte et al., 2025), which also explores interpolating between masked and uniform-noise diffusion. However, GIDD generally relies on constructing transition matrices that blend these mechanisms dynamically. In contrast, our XDLM framework enforces a stationary noise kernel. This design choice explicitly decouples the noise characteristics from the temporal dynamics, allowing us to derive a highly efficient scalar formulation that simplifies both sampling and training.

6. Conclusion

In this paper, we presented the XDLM, a unified approach that theoretically bridges the gap between Masked and Uniform-noise diffusion. By redefining the forward process as a weighted row-stochastic transition, we proved that XDLM recovers existing paradigms (MDLM and UDLM) as special cases. To ensure practicality, we derived a memory-efficient implementation that reduces computational complexity, enabling training on large vocabularies.

Empirically, XDLM breaks the Pareto frontier between understanding and generation. We identified a mixing ratio of $k = 0.1$ as the optimal “sweet spot”, where the model combines the robust zero-shot likelihoods of masking models with the superior sample diversity and few-step generation quality of uniform noise models. These advantages extend across domains, achieving state-of-the-art on ImageNet-1K and demonstrating significant scalability in the continual pretraining of 8B-parameter LLMs, where XDLM doubled performance on code generation benchmarks.

Limitations Despite these contributions, several avenues for future research remain. First, we have not yet trained XDLM from scratch at a large scale; such pre-training would likely allow for a more comprehensive exploration of the model’s emergent properties. Second, we did not fully investigate the “performance crossover” phenomenon, wherein UDLM and XDLM appear to outperform MDLM in generation tasks involving large sampling steps (approaching autoregressive decoding). Third, domain-specific sampling strategies for XDLM in language modeling and image generation have not yet been optimized. Furthermore, while we confirmed that XDLM balances understanding and generation, the interaction and balance between textual and visual modalities within a single unified model remain uninvestigated. Finally, the development of post-training schemas and inference acceleration techniques for XDLM remains a subject for future work.

Impact Statement

The primary objective of this research is to advance the technical state-of-the-art in machine learning. Consequently, it entails societal considerations parallel to those found in the general field of language and foundation models.

References

Austin, J., Johnson, D. D., Ho, J., Tarlow, D., and Van Den Berg, R. Structured denoising diffusion models in discrete state-spaces. *NeurIPS*, 34:17981–17993, 2021.

Campbell, A., Benton, J., De Bortoli, V., Rainforth, T., Deligiannidis, G., and Doucet, A. A continuous time framework for discrete denoising models. *NeurIPS*, 35: 28266–28279, 2022.

Chelba, C., Mikolov, T., Schuster, M., Ge, Q., Brants, T., Koehn, P., and Robinson, T. One billion word benchmark for measuring progress in statistical language modeling. *arXiv preprint arXiv:1312.3005*, 2013.

Cohan, A., Dernoncourt, F., Kim, D. S., Bui, T., Kim, S., Chang, W., and Goharian, N. A discourse-aware attention model for abstractive summarization of long documents. *arXiv preprint arXiv:1804.05685*, 2018.

Deng, J., Dong, W., Socher, R., Li, L.-J., Li, K., and Fei-Fei, L. Imagenet: A large-scale hierarchical image database. In *IEEE CVPR*, pp. 248–255. Ieee, 2009.

Devlin, J., Chang, M.-W., Lee, K., and Toutanova, K. Bert: Pre-training of deep bidirectional transformers for language understanding. In *NAACL*, pp. 4171–4186, 2019.

Dhariwal, P. and Nichol, A. Diffusion models beat gans on image synthesis. *NeurIPS*, 34:8780–8794, 2021.

Fathi, N., Scholak, T., and Noël, P.-A. Unifying autoregressive and diffusion-based sequence generation. *arXiv preprint arXiv:2504.06416*, 2025.

Gokaslan, A. and Cohen, V. Openwebtext corpus. <http://Skylion007.github.io/OpenWebTextCorpus>, 2019.

Gulrajani, I. and Hashimoto, T. B. Likelihood-based diffusion language models. *NeurIPS*, 36:16693–16715, 2023.

Ho, J., Jain, A., and Abbeel, P. Denoising diffusion probabilistic models. *NeurIPS*, 33:6840–6851, 2020.

Hoogeboom, E., Nielsen, D., Jaini, P., Forré, P., and Welling, M. Argmax flows and multinomial diffusion: Learning categorical distributions. *NeurIPS*, 34:12454–12465, 2021.

Kong, Z., Ping, W., Huang, J., Zhao, K., and Catanzaro, B. Diffwave: A versatile diffusion model for audio synthesis. *arXiv preprint arXiv:2009.09761*, 2020.

Krizhevsky, A., Hinton, G., et al. Learning multiple layers of features from tiny images. 2009.

Lipman, Y., Chen, R. T., Ben-Hamu, H., Nickel, M., and Le, M. Flow matching for generative modeling. *arXiv preprint arXiv:2210.02747*, 2022.

Lou, A., Meng, C., and Ermon, S. Discrete diffusion language modeling by estimating the ratios of the data distribution. 2023.

Marcus, M., Santorini, B., and Marcinkiewicz, M. A. Building a large annotated corpus of english: The penn treebank. *Computational linguistics*, 19(2):313–330, 1993.

Merity, S., Xiong, C., Bradbury, J., and Socher, R. Pointer sentinel mixture models. *arXiv preprint arXiv:1609.07843*, 2016.

Nie, S., Zhu, F., You, Z., Zhang, X., Ou, J., Hu, J., Zhou, J., Lin, Y., Wen, J.-R., and Li, C. Large language diffusion models. *arXiv preprint arXiv:2502.09992*, 2025.

Paperno, D., Kruszewski, G., Lazaridou, A., Pham, N.-Q., Bernardi, R., Pezzelle, S., Baroni, M., Boleda, G., and Fernández, R. The lambada dataset: Word prediction requiring a broad discourse context. In *ACL*, pp. 1525–1534, 2016.

Peebles, W. and Xie, S. Scalable diffusion models with transformers. In *IEEE ICCV*, pp. 4195–4205, 2023.

Penedo, G., Kydlíček, H., Lozhkov, A., Mitchell, M., Rafel, C. A., Von Werra, L., Wolf, T., et al. The fineweb datasets: Decanting the web for the finest text data at scale. *NeurIPS*, 37:30811–30849, 2024.

Radford, A., Wu, J., Child, R., Luan, D., Amodei, D., Sutskever, I., et al. Language models are unsupervised multitask learners. *OpenAI blog*, 1(8):9, 2019.

Rombach, R., Blattmann, A., Lorenz, D., Esser, P., and Ommer, B. High-resolution image synthesis with latent diffusion models. In *IEEE CVPR*, pp. 10684–10695, 2022.

Ronneberger, O., Fischer, P., and Brox, T. U-net: Convolutional networks for biomedical image segmentation. In *MICCAI*, pp. 234–241. Springer, 2015.

Sahoo, S., Arriola, M., Schiff, Y., Gokaslan, A., Marroquin, E., Chiu, J., Rush, A., and Kuleshov, V. Simple and effective masked diffusion language models. *NeurIPS*, 37:130136–130184, 2024.

Sahoo, S. S., Deschenaux, J., Gokaslan, A., Wang, G., Chiu, J., and Kuleshov, V. The diffusion duality. *arXiv preprint arXiv:2506.10892*, 2025.

Schiff, Y., Sahoo, S. S., Phung, H., Wang, G., Boshar, S., Dalla-torre, H., de Almeida, B. P., Rush, A. M., PIER-ROT, T., and Kuleshov, V. Simple guidance mechanisms for discrete diffusion models. In *ICLR*, 2024.

Shi, J., Han, K., Wang, Z., Doucet, A., and Titsias, M. Simplified and generalized masked diffusion for discrete data. *NeurIPS*, 37:103131–103167, 2024.

Sun, P., Jiang, Y., Chen, S., Zhang, S., Peng, B., Luo, P., and Yuan, Z. Autoregressive model beats diffusion: Llama for scalable image generation. *arXiv preprint arXiv:2406.06525*, 2024.

von Rütte, D., Fluri, J., Ding, Y., Orvieto, A., Schölkopf, B., and Hofmann, T. Generalized interpolating discrete diffusion. *arXiv preprint arXiv:2503.04482*, 2025.

Wang, G., Schiff, Y., Sahoo, S. S., and Kuleshov, V. Remasking discrete diffusion models with inference-time scaling. *arXiv preprint arXiv:2503.00307*, 2025.

Yang, L., Tian, Y., Li, B., Zhang, X., Shen, K., Tong, Y., and Wang, M. Mmada: Multimodal large diffusion language models. *arXiv preprint arXiv:2505.15809*, 2025.

Ye, J., Xie, Z., Zheng, L., Gao, J., Wu, Z., Jiang, X., Li, Z., and Kong, L. Dream 7b: Diffusion large language models. *arXiv preprint arXiv:2508.15487*, 2025.

You, Z., Nie, S., Zhang, X., Hu, J., Zhou, J., Lu, Z., Wen, J.-R., and Li, C. Llada-v: Large language diffusion models with visual instruction tuning. *arXiv preprint arXiv:2505.16933*, 2025.

Yu, R., Ma, X., and Wang, X. Dimple: Discrete diffusion multimodal large language model with parallel decoding. *arXiv preprint arXiv:2505.16990*, 2025.

Zhang, X., Zhao, J., and LeCun, Y. Character-level convolutional networks for text classification. *NeurIPS*, 28, 2015.

A. The Forward Process with Stationary Kernels

Lemma 1 (Construction of Mixing Kernel). *Let $\pi \in \mathcal{R}^N$ be a stationary target distribution defined as a mixture of the uniform distribution \mathbf{u} and point-masses on special tokens $i \in \mathcal{S}$. If the noise kernel \mathbf{K} satisfies the property of instantaneous mixing (i.e., convergence to π in a single step), it admits the decomposition:*

$$\mathbf{K} = \frac{k}{N} \mathbf{J} + \sum_{i \in \mathcal{S}} \mu_i \mathbf{M}_i, \quad (20)$$

where \mathbf{J} is the all-ones matrix, \mathbf{M}_i is the absorbing matrix for state i , and the weights satisfy $k + \sum \mu_i = 1$.

Proof. The condition of instantaneous mixing implies that the transition probability to a destination state j is solely determined by the target marginal π_j , independent of the antecedent state s . In terms of the stochastic matrix, this imposes row-equivalence: $\mathbf{K}_{sj} = \pi_j$ for all s . This is algebraically equivalent to the rank-1 factorization $\mathbf{K} = \mathbf{1}\pi^\top$.

Substituting the mixture definition $\pi = k\mathbf{u} + \sum_{i \in \mathcal{S}} \mu_i \mathbf{e}_i$ into this factorization yields:

$$\mathbf{K} = \mathbf{1} \left(k\mathbf{u} + \sum_{i \in \mathcal{S}} \mu_i \mathbf{e}_i \right)^\top \quad (21)$$

$$= k(\mathbf{1}\mathbf{u}^\top) + \sum_{i \in \mathcal{S}} \mu_i (\mathbf{1}\mathbf{e}_i^\top). \quad (22)$$

Identifying the resulting outer products with the canonical transition matrices $\mathbf{1}\mathbf{u}^\top = N^{-1}\mathbf{J}$ (uniform transition) and $\mathbf{1}\mathbf{e}_i^\top = \mathbf{M}_i$ (absorbing transition) concludes the proof. \square

B. Efficient Sampling and Training via Scalar Formulation

Before proofing `lemma`, we introduce this definition:

Definition B.1.

$$\mathbf{g}(s, t, \mathbf{x}, \mathbf{z}_t) \quad (23)$$

$$= \alpha_t \mathbf{z}_t \odot \mathbf{x} + \alpha_{t|s} \beta_s \mathbf{z}_t \odot K^\top \mathbf{x} + \beta_{t|s} \alpha_s K \mathbf{z}_t \odot \mathbf{x} + \beta_{t|s} \beta_s K \mathbf{z}_t \odot K^\top \mathbf{x} \quad (24)$$

$$= \alpha_{t|s} f_s(\mathbf{x}, \mathbf{z}_t) \mathbf{z}_t + \beta_{t|s} r(\mathbf{z}_t) \left(\alpha_s \mathbf{x} + \beta_s \left(\frac{k}{N} \mathbf{1} + \mu \mathbf{m} \right) \right) \quad (25)$$

Thus, we have

$$\mathbf{e}^\top \mathbf{g}(s, t, \mathbf{x}, \mathbf{z}_t) \quad (26)$$

$$= \alpha_{t|s} f_s(\mathbf{x}, \mathbf{z}_t) \mathbf{e}^\top \mathbf{z}_t + \beta_{t|s} r(\mathbf{z}_t) \left(\alpha_s \mathbf{e}^\top \mathbf{x} + \beta_s \left(\frac{k}{N} \mathbf{e}^\top \mathbf{1} + \mu \mathbf{e}^\top \mathbf{m} \right) \right) \quad (27)$$

$$= f_s(\mathbf{x}, \mathbf{z}_t) \alpha_{t|s} \mathbf{e}^\top \mathbf{z}_t + \beta_{t|s} r(\mathbf{z}_t) (\alpha_s \mathbf{e}^\top \mathbf{x} + \beta_s r(\mathbf{e})) \quad (28)$$

$$= f_s(\mathbf{x}, \mathbf{e}) \alpha_{t|s} \mathbf{e}^\top \mathbf{z}_t + \beta_{t|s} r(\mathbf{z}_t) f_s(\mathbf{x}, \mathbf{e}) \quad (29)$$

$$= f_s(\mathbf{x}, \mathbf{e}) f_{t|s}(\mathbf{e}, \mathbf{z}_t) \quad (30)$$

Lemma 2 (Scalar Posterior). *The posterior probability of transitioning to state \mathbf{e} can be formulated as:*

$$q(\mathbf{z}_s = \mathbf{e} \mid \mathbf{z}_t, \mathbf{x}) = \frac{f_s(\mathbf{x}, \mathbf{e}) f_{t|s}(\mathbf{e}, \mathbf{z}_t)}{f_t(\mathbf{x}, \mathbf{z}_t)}. \quad (31)$$

The model's reverse transition p_θ follows the same form by substituting \mathbf{x} with the predicted distribution $\tilde{\mathbf{x}}_0$.

Proof.

$$q(\mathbf{z}_s = \mathbf{e} | \mathbf{z}_t, \mathbf{x}) \quad (32)$$

$$= \mathbf{e}^\top \frac{(Q_{t|s} \mathbf{z}_t) \odot (Q_s^\top \mathbf{x})}{\mathbf{z}_t^\top Q_t^\top \mathbf{x}} \quad (33)$$

$$= \mathbf{e}^\top \frac{(\alpha_{t|s} \mathbf{z}_t + \beta_{t|s} K \mathbf{z}_t) \odot (\alpha_s \mathbf{x} + \beta_s K^\top \mathbf{x})}{\mathbf{z}_t^\top (\alpha_t \mathbf{x} + \beta_t K^\top \mathbf{x})} \quad (34)$$

$$= \mathbf{e}^\top \frac{\alpha_t \mathbf{z}_t \odot \mathbf{x} + \alpha_{t|s} \beta_s \mathbf{z}_t \odot K^\top \mathbf{x} + \beta_{t|s} \alpha_s K \mathbf{z}_t \odot \mathbf{x} + \beta_{t|s} \beta_s K \mathbf{z}_t \odot K^\top \mathbf{x}}{\alpha_t \mathbf{z}_t^\top \mathbf{x} + \beta_t \mathbf{z}_t^\top K^\top \mathbf{x}} \quad (35)$$

$$= \mathbf{e}^\top \frac{\mathbf{g}(s, t, \mathbf{x}, \mathbf{z}_t)}{f_t(\mathbf{x}, \mathbf{z}_t)} \quad (36)$$

$$= \frac{f_s(\mathbf{x}, \mathbf{e}) f_{t|s}(\mathbf{e}, \mathbf{z}_t)}{f_t(\mathbf{x}, \mathbf{z}_t)} \quad (37)$$

□

Lemma 3 (Scalar KL Divergence). *The term $D_{KL}(q(\mathbf{z}_s | \mathbf{z}_t, \mathbf{x}) \parallel p_\theta(\mathbf{z}_s | \mathbf{z}_t))$ can be written as:*

$$D_{KL} = \frac{\beta_{t|s} \alpha_s r(\mathbf{z}_t)}{f_t(\mathbf{x}, \mathbf{z}_t)} h_t(\mathbf{x}, \mathbf{z}_t, \tilde{\mathbf{x}}_0), \quad (38)$$

where h_t is an auxiliary function collecting the logarithmic difference terms:

$$\begin{aligned} h_t(\mathbf{x}, \mathbf{z}_t, \tilde{\mathbf{x}}_0) &= \frac{f_s(\mathbf{x}, \mathbf{z}_t)}{r(\mathbf{z}_t)} \frac{\alpha_{t|s}}{\beta_{t|s} \alpha_s} \log \frac{f_s(\mathbf{x}, \mathbf{z}_t) f_t(\tilde{\mathbf{x}}_0, \mathbf{z}_t)}{f_t(\mathbf{x}, \mathbf{z}_t) f_s(\tilde{\mathbf{x}}_0, \mathbf{z}_t)} \\ &\quad - \frac{1}{\alpha_s} \log \frac{f_t(\mathbf{x}, \mathbf{z}_t)}{f_t(\tilde{\mathbf{x}}_0, \mathbf{z}_t)} + \log \frac{f_s(\mathbf{x}, \mathbf{x})}{f_s(\tilde{\mathbf{x}}_0, \mathbf{x})} \\ &\quad + \frac{k \beta_s}{N \alpha_s} \sum_{\mathbf{e} \in \mathcal{V}} \log \frac{f_s(\mathbf{x}, \mathbf{e})}{f_s(\tilde{\mathbf{x}}_0, \mathbf{e})}. \end{aligned} \quad (39)$$

Proof.

$$D_{KL} = \sum_{\mathbf{e}} q(\mathbf{z}_s = \mathbf{e} | \mathbf{z}_t, \mathbf{x}) \log \frac{q(\mathbf{z}_s = \mathbf{e} | \mathbf{z}_t, \mathbf{x})}{p_{\theta}(\mathbf{z}_s = \mathbf{e} | \mathbf{z}_t)} \quad (40)$$

$$= \sum_{\mathbf{e}} q(\mathbf{z}_s = \mathbf{e} | \mathbf{z}_t, \mathbf{x}) \log \frac{q(\mathbf{z}_s = \mathbf{e} | \mathbf{z}_t, \mathbf{x})}{q(\mathbf{z}_s = \mathbf{e} | \mathbf{z}_t, \tilde{\mathbf{x}}_0)} \quad (41)$$

$$= \sum_{\mathbf{e}} \frac{f_s(\mathbf{x}, \mathbf{e}) f_{t|s}(\mathbf{e}, \mathbf{z}_t)}{f_t(\mathbf{x}, \mathbf{z}_t)} \left(\log \frac{f_s(\mathbf{x}, \mathbf{e}) f_{t|s}(\mathbf{e}, \mathbf{z}_t)}{f_t(\mathbf{x}, \mathbf{z}_t)} - \log \frac{f_s(\tilde{\mathbf{x}}_0, \mathbf{e}) f_{t|s}(\mathbf{e}, \mathbf{z}_t)}{f_t(\tilde{\mathbf{x}}_0, \mathbf{z}_t)} \right) \quad (42)$$

$$= \frac{1}{f_t(\mathbf{x}, \mathbf{z}_t)} \sum_{\mathbf{e}} f_s(\mathbf{x}, \mathbf{e}) f_{t|s}(\mathbf{e}, \mathbf{z}_t) \log \frac{f_s(\mathbf{x}, \mathbf{e}) f_t(\tilde{\mathbf{x}}_0, \mathbf{z}_t)}{f_t(\mathbf{x}, \mathbf{z}_t) f_s(\tilde{\mathbf{x}}_0, \mathbf{e})} \quad (43)$$

$$= \frac{1}{f_t(\mathbf{x}, \mathbf{z}_t)} \sum_{\mathbf{e}} f_s(\mathbf{x}, \mathbf{e}) (\alpha_{t|s} \delta_{\mathbf{e}, \mathbf{z}_t} + \beta_{t|s} r(\mathbf{z}_t)) \log \frac{f_s(\mathbf{x}, \mathbf{e}) f_t(\tilde{\mathbf{x}}_0, \mathbf{z}_t)}{f_t(\mathbf{x}, \mathbf{z}_t) f_s(\tilde{\mathbf{x}}_0, \mathbf{e})} \quad (44)$$

$$= \frac{\alpha_{t|s} f_s(\mathbf{x}, \mathbf{z}_t)}{f_t(\mathbf{x}, \mathbf{z}_t)} \log \frac{f_s(\mathbf{x}, \mathbf{z}_t) f_t(\tilde{\mathbf{x}}_0, \mathbf{z}_t)}{f_t(\mathbf{x}, \mathbf{z}_t) f_s(\tilde{\mathbf{x}}_0, \mathbf{z}_t)} \quad (45)$$

$$+ \frac{\beta_{t|s} r(\mathbf{z}_t)}{f_t(\mathbf{x}, \mathbf{z}_t)} \log \frac{f_t(\tilde{\mathbf{x}}_0, \mathbf{z}_t)}{f_t(\mathbf{x}, \mathbf{z}_t)} \sum_{\mathbf{e}} f_s(\mathbf{x}, \mathbf{e}) \quad (46)$$

$$+ \frac{\beta_{t|s} r(\mathbf{z}_t)}{f_t(\mathbf{x}, \mathbf{z}_t)} \sum_{\mathbf{e}} f_s(\mathbf{x}, \mathbf{e}) \log \frac{f_s(\mathbf{x}, \mathbf{e})}{f_s(\tilde{\mathbf{x}}_0, \mathbf{e})} \quad (47)$$

$$= \frac{\alpha_{t|s} f_s(\mathbf{x}, \mathbf{z}_t)}{f_t(\mathbf{x}, \mathbf{z}_t)} \log \frac{f_s(\mathbf{x}, \mathbf{z}_t) f_t(\tilde{\mathbf{x}}_0, \mathbf{z}_t)}{f_t(\mathbf{x}, \mathbf{z}_t) f_s(\tilde{\mathbf{x}}_0, \mathbf{z}_t)} - \frac{\beta_{t|s} r(\mathbf{z}_t)}{f_t(\mathbf{x}, \mathbf{z}_t)} \log \frac{f_t(\mathbf{x}, \mathbf{z}_t)}{f_t(\tilde{\mathbf{x}}_0, \mathbf{z}_t)} \quad (48)$$

$$+ \frac{\beta_{t|s} r(\mathbf{z}_t)}{f_t(\mathbf{x}, \mathbf{z}_t)} \sum_{\mathbf{e}} (\alpha_s \delta_{\mathbf{x}, \mathbf{e}} + \beta_s r(\mathbf{e})) \log \frac{f_s(\mathbf{x}, \mathbf{e})}{f_s(\tilde{\mathbf{x}}_0, \mathbf{e})} \quad (49)$$

$$= \frac{\alpha_{t|s} f_s(\mathbf{x}, \mathbf{z}_t)}{f_t(\mathbf{x}, \mathbf{z}_t)} \log \frac{f_s(\mathbf{x}, \mathbf{z}_t) f_t(\tilde{\mathbf{x}}_0, \mathbf{z}_t)}{f_t(\mathbf{x}, \mathbf{z}_t) f_s(\tilde{\mathbf{x}}_0, \mathbf{z}_t)} - \frac{\beta_{t|s} r(\mathbf{z}_t)}{f_t(\mathbf{x}, \mathbf{z}_t)} \log \frac{f_t(\mathbf{x}, \mathbf{z}_t)}{f_t(\tilde{\mathbf{x}}_0, \mathbf{z}_t)} \quad (50)$$

$$+ \frac{\beta_{t|s} \alpha_s r(\mathbf{z}_t)}{f_t(\mathbf{x}, \mathbf{z}_t)} \log \frac{f_s(\mathbf{x}, \mathbf{x})}{f_s(\tilde{\mathbf{x}}_0, \mathbf{x})} \quad (51)$$

$$+ \frac{k \beta_{t|s} \beta_s r(\mathbf{z}_t)}{N f_t(\mathbf{x}, \mathbf{z}_t)} \sum_{\mathbf{e}} \log \frac{f_s(\mathbf{x}, \mathbf{e})}{f_s(\tilde{\mathbf{x}}_0, \mathbf{e})} + \frac{\mu \beta_{t|s} \beta_s r(\mathbf{z}_t)}{f_t(\mathbf{x}, \mathbf{z}_t)} \log \frac{f_s(\mathbf{x}, \mathbf{m})}{f_s(\tilde{\mathbf{x}}_0, \mathbf{m})} \quad (52)$$

$$= \frac{\beta_{t|s} \alpha_s r(\mathbf{z}_t)}{f_t(\mathbf{x}, \mathbf{z}_t)} h_t(\mathbf{x}, \mathbf{z}_t) \quad (53)$$

We omit the term $\log f_s(\mathbf{x}, \mathbf{m}) / f_s(\tilde{\mathbf{x}}_0, \mathbf{m})$ as it equals zero for all \mathbf{x} and $\tilde{\mathbf{x}}_0$.

□

Lemma 4 (Limiting Case). *As $s \rightarrow t$, the function h_t converges to:*

$$\begin{aligned} h_t(\mathbf{x}, \mathbf{z}_t, \tilde{\mathbf{x}}_0) &\approx \frac{p_{\mathbf{x}, \mathbf{z}_t} - p_{\tilde{\mathbf{x}}_0, \mathbf{z}_t}}{f_t(\tilde{\mathbf{x}}_0, \mathbf{z}_t)} - \frac{1}{\alpha_t} \log \frac{f_t(\mathbf{x}, \mathbf{z}_t)}{f_t(\tilde{\mathbf{x}}_0, \mathbf{z}_t)} + \\ &\log \frac{f_t(\mathbf{x}, \mathbf{x})}{f_t(\tilde{\mathbf{x}}_0, \mathbf{x})} + \frac{k \beta_t}{N \alpha_t} \sum_{\mathbf{e} \in \mathcal{V}} \log \frac{f_t(\mathbf{x}, \mathbf{e})}{f_t(\tilde{\mathbf{x}}_0, \mathbf{e})}. \end{aligned} \quad (54)$$

Proof. Notice that when $s \rightarrow t$, $\beta_{t|s} \alpha_s \rightarrow 0$, which is a 0/0 div. by applying L'Hôpital's rule. (the up and down both

differentiate by $\alpha_{t|s}$), we have

$$\lim_{s \rightarrow t} \frac{1}{\beta_{t|s} \alpha_s} \log \frac{f_s(\mathbf{x}, \mathbf{z}_t) f_t(\tilde{\mathbf{x}}_0, \mathbf{z}_t)}{f_t(\mathbf{x}, \mathbf{z}_t) f_s(\tilde{\mathbf{x}}_0, \mathbf{z}_t)} \quad (55)$$

$$= \frac{-1}{\alpha_s} \frac{\partial}{\partial \alpha_{t|s}} \log \frac{f_s(\mathbf{x}, \mathbf{z}_t) f_t(\tilde{\mathbf{x}}_0, \mathbf{z}_t)}{f_t(\mathbf{x}, \mathbf{z}_t) f_s(\tilde{\mathbf{x}}_0, \mathbf{z}_t)} \quad (56)$$

$$= \frac{-1}{\alpha_s} \left(\frac{\partial \log f_s(\mathbf{x}, \mathbf{z}_t) f_t(\tilde{\mathbf{x}}_0, \mathbf{z}_t)}{\partial \alpha_{t|s}} - \frac{\partial \log f_t(\mathbf{x}, \mathbf{z}_t) f_s(\tilde{\mathbf{x}}_0, \mathbf{z}_t)}{\partial \alpha_{t|s}} \right) \quad (57)$$

$$= \frac{-1}{\alpha_s} \left(\frac{\partial \log f_t(\tilde{\mathbf{x}}_0, \mathbf{z}_t)}{\partial \alpha_{t|s}} - \frac{\partial \log f_t(\mathbf{x}, \mathbf{z}_t)}{\partial \alpha_{t|s}} \right) \quad (58)$$

$$= \frac{-1}{\alpha_s} \left(\frac{1}{f_t(\tilde{\mathbf{x}}_0, \mathbf{z}_t)} \frac{\partial(\alpha_t p_{\tilde{\mathbf{x}}_0, \mathbf{z}_t} + (1 - \alpha_t)r(\mathbf{z}_t))}{\partial \alpha_{t|s}} - \frac{1}{f_t(\mathbf{x}, \mathbf{z}_t)} \frac{\partial f_t(\mathbf{x}, \mathbf{z}_t)}{\partial \alpha_{t|s}} \right) \quad (59)$$

$$= \frac{-1}{\alpha_s} \left(\frac{1}{f_t(\tilde{\mathbf{x}}_0, \mathbf{z}_t)} (\alpha_s p_{\tilde{\mathbf{x}}_0, \mathbf{z}_t} - \alpha_s r(\mathbf{z}_t)) - \frac{1}{f_t(\mathbf{x}, \mathbf{z}_t)} \frac{\partial f_t(\mathbf{x}, \mathbf{z}_t)}{\partial \alpha_{t|s}} \right) \quad (60)$$

$$= -\frac{p_{\tilde{\mathbf{x}}_0, \mathbf{z}_t} - r(\mathbf{z}_t)}{f_t(\tilde{\mathbf{x}}_0, \mathbf{z}_t)} + \frac{p_{\mathbf{x}, \mathbf{z}_t} - r(\mathbf{z}_t)}{f_t(\mathbf{x}, \mathbf{z}_t)} \quad (61)$$

$$= \frac{(\alpha_t p_{\tilde{\mathbf{x}}_0, \mathbf{z}_t} + \beta_t r(\mathbf{z}_t))(p_{\mathbf{x}, \mathbf{z}_t} - r(\mathbf{z}_t)) - (\alpha_t p_{\mathbf{x}, \mathbf{z}_t} + \beta_t r(\mathbf{z}_t))(p_{\tilde{\mathbf{x}}_0, \mathbf{z}_t} - r(\mathbf{z}_t))}{f_t(\mathbf{x}, \mathbf{z}_t) f_t(\tilde{\mathbf{x}}_0, \mathbf{z}_t)} \quad (62)$$

$$= \frac{-\alpha_t p_{\tilde{\mathbf{x}}_0, \mathbf{z}_t} r(\mathbf{z}_t) + \beta_t p_{\mathbf{x}, \mathbf{z}_t} r(\mathbf{z}_t) + \alpha_t p_{\mathbf{x}, \mathbf{z}_t} r(\mathbf{z}_t) - \beta_t p_{\tilde{\mathbf{x}}_0, \mathbf{z}_t} r(\mathbf{z}_t)}{f_t(\mathbf{x}, \mathbf{z}_t) f_t(\tilde{\mathbf{x}}_0, \mathbf{z}_t)} \quad (63)$$

$$= \frac{r(\mathbf{z}_t)(p_{\mathbf{x}, \mathbf{z}_t} - p_{\tilde{\mathbf{x}}_0, \mathbf{z}_t})}{f_t(\mathbf{x}, \mathbf{z}_t) f_t(\tilde{\mathbf{x}}_0, \mathbf{z}_t)} \quad (64)$$

so

$$\lim_{s \rightarrow t} \left(\frac{f_s(\mathbf{x}, \mathbf{z}_t)}{r(\mathbf{z}_t)} \frac{\alpha_{t|s}}{\beta_{t|s} \alpha_s} \log \frac{f_s(\mathbf{x}, \mathbf{z}_t) f_t(\tilde{\mathbf{x}}_0, \mathbf{z}_t)}{f_t(\mathbf{x}, \mathbf{z}_t) f_s(\tilde{\mathbf{x}}_0, \mathbf{z}_t)} \right) = \frac{p_{\mathbf{x}, \mathbf{z}_t} - p_{\tilde{\mathbf{x}}_0, \mathbf{z}_t}}{f_t(\tilde{\mathbf{x}}_0, \mathbf{z}_t)} \quad (65)$$

□

C. Relationship to MDLM and UDLM

Lemma 5. *XDLM can be reduced to MDLM by setting $k = 0$, with the posterior probability:*

$$p_\theta(\mathbf{z}_s = \mathbf{e} | \mathbf{z}_t) = \delta_{\mathbf{z}_t, \mathbf{m}} \delta_{\mathbf{e}, \mathbf{m}} \frac{\beta_s}{\beta_t} + \delta_{\mathbf{z}_t, \mathbf{m}} \delta_{\mathbf{e} \neq \mathbf{m}} \frac{\beta_{t|s} \alpha_s p_{\theta, \mathbf{e}}}{\beta_t} + \delta_{\mathbf{z}_t \neq \mathbf{m}} \delta_{\mathbf{e}, \mathbf{z}_t} \quad (66)$$

$$= \begin{cases} \frac{\beta_s}{\beta_t} \delta_{\mathbf{m}, \mathbf{z}_t}, & \mathbf{e} = \mathbf{m} \\ \frac{(\alpha_s - \alpha_t)}{1 - \alpha_t} p_{\theta, \mathbf{e}}, & \mathbf{z}_t = \mathbf{m}, \mathbf{e} \neq \mathbf{m} \\ \delta_{\mathbf{e}, \mathbf{z}_t}, & \mathbf{z}_t \neq \mathbf{m}, \mathbf{e} \neq \mathbf{m} \end{cases} \quad (67)$$

and kl divergence

$$KL = -\frac{\beta_{t|s} \alpha_s}{\beta_t} \log p_{\theta, \mathbf{x}} \quad (68)$$

Proof. since $k = 0$, $\mu = 1$, we have

$$r(\mathbf{e}) = \delta_{\mathbf{e}, \mathbf{m}} \quad (69)$$

$$p_{\tilde{\mathbf{x}}_0, \mathbf{e}} = \delta_{\mathbf{e} \neq \mathbf{m}} p_{\tilde{\mathbf{x}}_0, \mathbf{e}} \quad (70)$$

hence

$$q(\mathbf{z}_s = \mathbf{e} | \mathbf{z}_t, \tilde{\mathbf{x}}_0) = \frac{f_s(\tilde{\mathbf{x}}_0, \mathbf{e}) f_{t|s}(\mathbf{e}, \mathbf{z}_t)}{f_t(\tilde{\mathbf{x}}_0, \mathbf{z}_t)} \quad (71)$$

$$= \frac{(\alpha_s p_{\tilde{\mathbf{x}}_0, \mathbf{e}} + \beta_s r(\mathbf{e})) (\alpha_{t|s} p_{\mathbf{e}, \mathbf{z}_t} + \beta_{t|s} r(\mathbf{z}_t))}{\alpha_t p_{\tilde{\mathbf{x}}_0, \mathbf{z}_t} + \beta_t r(\mathbf{z}_t)} \quad (72)$$

$$= \frac{\alpha_t p_{\tilde{\mathbf{x}}_0, \mathbf{e}} \delta_{\mathbf{e}, \mathbf{z}_t} + \alpha_s \beta_{t|s} p_{\tilde{\mathbf{x}}_0, \mathbf{e}} \delta_{\mathbf{z}_t, \mathbf{m}} + \alpha_{t|s} \beta_s \delta_{\mathbf{e}, \mathbf{z}_t} \delta_{\mathbf{e}, \mathbf{m}} + \beta_s \beta_{t|s} \delta_{\mathbf{e}, \mathbf{m}} \delta_{\mathbf{z}_t, \mathbf{m}}}{\alpha_t p_{\tilde{\mathbf{x}}_0, \mathbf{z}_t} + \beta_t \delta_{\mathbf{z}_t, \mathbf{m}}} \quad (73)$$

$$= \delta_{\mathbf{z}_t, \mathbf{m}} \frac{\alpha_s \beta_{t|s} p_{\tilde{\mathbf{x}}_0, \mathbf{e}} + \alpha_{t|s} \beta_s \delta_{\mathbf{e}, \mathbf{z}_t} + \beta_s \beta_{t|s} \delta_{\mathbf{e}, \mathbf{z}_t}}{\beta_t} \quad (74)$$

$$+ \delta_{\mathbf{z}_t \neq \mathbf{m}} \frac{\alpha_t p_{\tilde{\mathbf{x}}_0, \mathbf{e}} \delta_{\mathbf{e}, \mathbf{z}_t}}{\alpha_t p_{\tilde{\mathbf{x}}_0, \mathbf{z}_t}} \quad (75)$$

$$= \delta_{\mathbf{z}_t, \mathbf{m}} \left(\frac{\alpha_s \beta_{t|s}}{\beta_t} p_{\tilde{\mathbf{x}}_0, \mathbf{e}} + \frac{\beta_s}{\beta_t} \delta_{\mathbf{e}, \mathbf{z}_t} \right) + \delta_{\mathbf{z}_t \neq \mathbf{m}} \delta_{\mathbf{e}, \mathbf{z}_t} \frac{p_{\tilde{\mathbf{x}}_0, \mathbf{e}}}{p_{\tilde{\mathbf{x}}_0, \mathbf{z}_t}} \quad (76)$$

$$= \delta_{\mathbf{z}_t, \mathbf{m}} \frac{\alpha_s \beta_{t|s}}{\beta_t} p_{\tilde{\mathbf{x}}_0, \mathbf{e}} + \frac{\beta_s}{\beta_t} \delta_{\mathbf{z}_t, \mathbf{m}} \delta_{\mathbf{e}, \mathbf{z}_t} + \delta_{\mathbf{z}_t \neq \mathbf{m}} \delta_{\mathbf{e}, \mathbf{z}_t} \quad (77)$$

for kl, we have

$$h_t(\mathbf{x}, \mathbf{z}_t) = \frac{f_s(\mathbf{x}, \mathbf{z}_t)}{r(\mathbf{z}_t)} \frac{\alpha_{t|s}}{\beta_{t|s} \alpha_s} \log \frac{f_s(\mathbf{x}, \mathbf{z}_t) f_t(\tilde{\mathbf{x}}_0, \mathbf{z}_t)}{f_t(\mathbf{x}, \mathbf{z}_t) f_s(\tilde{\mathbf{x}}_0, \mathbf{z}_t)} \quad (78)$$

$$- \frac{1}{\alpha_s} \log \frac{f_t(\mathbf{x}, \mathbf{z}_t)}{f_t(\tilde{\mathbf{x}}_0, \mathbf{z}_t)} + \log \frac{f_s(\mathbf{x}, \mathbf{x})}{f_s(\tilde{\mathbf{x}}_0, \mathbf{x})} + \frac{k \beta_s}{N \alpha_s} \sum_{\mathbf{e}} \log \frac{f_s(\mathbf{x}, \mathbf{e})}{f_s(\tilde{\mathbf{x}}_0, \mathbf{e})} \quad (79)$$

$$= \frac{f_s(\mathbf{x}, \mathbf{z}_t)}{r(\mathbf{z}_t)} \frac{\alpha_{t|s}}{\beta_{t|s} \alpha_s} \log \frac{(\alpha_s p_{\mathbf{x}, \mathbf{z}_t} + \beta_s \delta_{\mathbf{z}_t, \mathbf{m}})(\alpha_t p_{\tilde{\mathbf{x}}_0, \mathbf{z}_t} + \beta_t \delta_{\mathbf{z}_t, \mathbf{m}})}{(\alpha_t p_{\mathbf{x}, \mathbf{z}_t} + \beta_t \delta_{\mathbf{z}_t, \mathbf{m}})(\alpha_s p_{\tilde{\mathbf{x}}_0, \mathbf{z}_t} + \beta_s \delta_{\mathbf{z}_t, \mathbf{m}})} \quad (80)$$

$$- \frac{1}{\alpha_s} \log \frac{\alpha_t p_{\mathbf{x}, \mathbf{z}_t} + \beta_t \delta_{\mathbf{z}_t, \mathbf{m}}}{\alpha_t p_{\tilde{\mathbf{x}}_0, \mathbf{z}_t} + \beta_t \delta_{\mathbf{z}_t, \mathbf{m}}} - \log p_{\tilde{\mathbf{x}}_0, \mathbf{x}} \quad (81)$$

$$= \frac{f_s(\mathbf{x}, \mathbf{z}_t)}{r(\mathbf{z}_t)} \frac{\alpha_{t|s}}{\beta_{t|s} \alpha_s} \log \left(\delta_{\mathbf{z}_t, \mathbf{m}} \frac{\beta_s \delta_{\mathbf{z}_t, \mathbf{m}} \beta_t \delta_{\mathbf{z}_t, \mathbf{m}}}{\beta_t \delta_{\mathbf{z}_t, \mathbf{m}} \beta_s \delta_{\mathbf{z}_t, \mathbf{m}}} + \delta_{\mathbf{z}_t \neq \mathbf{m}} \frac{\alpha_s p_{\mathbf{x}, \mathbf{z}_t} \alpha_t p_{\tilde{\mathbf{x}}_0, \mathbf{z}_t}}{\alpha_t p_{\mathbf{x}, \mathbf{z}_t} \alpha_s p_{\tilde{\mathbf{x}}_0, \mathbf{z}_t}} \right) \quad (82)$$

$$- \frac{1}{\alpha_s} \log \left(\delta_{\mathbf{z}_t, \mathbf{m}} \frac{\beta_t \delta_{\mathbf{z}_t, \mathbf{m}}}{\beta_t \delta_{\mathbf{z}_t, \mathbf{m}}} + \delta_{\mathbf{z}_t \neq \mathbf{m}} \frac{\alpha_t p_{\mathbf{x}, \mathbf{z}_t}}{\alpha_t p_{\tilde{\mathbf{x}}_0, \mathbf{z}_t}} \right) - \log p_{\tilde{\mathbf{x}}_0, \mathbf{x}} \quad (83)$$

$$= \frac{f_s(\mathbf{x}, \mathbf{z}_t)}{r(\mathbf{z}_t)} \frac{\alpha_{t|s}}{\beta_{t|s} \alpha_s} \log (1) - \frac{1}{\alpha_s} \delta_{\mathbf{z}_t \neq \mathbf{m}} \log \frac{p_{\mathbf{x}, \mathbf{z}_t}}{p_{\tilde{\mathbf{x}}_0, \mathbf{z}_t}} - \log p_{\tilde{\mathbf{x}}_0, \mathbf{x}} \quad (84)$$

so

$$D_{KL} = \frac{\beta_{t|s} \alpha_s r(\mathbf{z}_t)}{f_t(\mathbf{x}, \mathbf{z}_t)} h_t(\mathbf{x}, \mathbf{z}_t) \quad (85)$$

$$= - \frac{\beta_{t|s} \delta_{\mathbf{z}_t, \mathbf{m}}}{f_t(\mathbf{x}, \mathbf{z}_t)} \delta_{\mathbf{z}_t \neq \mathbf{m}} \log \frac{p_{\mathbf{x}, \mathbf{z}_t}}{p_{\tilde{\mathbf{x}}_0, \mathbf{z}_t}} - \frac{\beta_{t|s} \alpha_s \delta_{\mathbf{z}_t, \mathbf{m}}}{\alpha_t \delta_{\mathbf{x}, \mathbf{z}_t} + \beta_t \delta_{\mathbf{z}_t, \mathbf{m}}} \log p_{\tilde{\mathbf{x}}_0, \mathbf{x}} \quad (86)$$

$$= - \delta_{\mathbf{z}_t, \mathbf{m}} \frac{\beta_{t|s} \alpha_s}{\beta_t} \log p_{\tilde{\mathbf{x}}_0, \mathbf{x}} \quad (87)$$

□

Lemma 6. *XDLM can be reduced to UDLM by setting $k = 1$, with the posterior probability:*

$$p_{\theta}(\mathbf{z}_s = \mathbf{e} | \mathbf{z}_t) = \frac{\delta_{\mathbf{e}, \mathbf{z}_t} (N \alpha_t p_{\theta, \mathbf{e}} + \beta_s \alpha_{t|s}) + (\alpha_s - \alpha_t) p_{\theta, \mathbf{e}} + \beta_s \beta_{t|s} / N}{N \alpha_t p_{\theta, \mathbf{z}_t} + \beta_t} \quad (88)$$

and kl divergence

$$KL = \frac{-\beta_{t|s}\alpha_s}{N\alpha_t} \left(\frac{1}{f_t(\tilde{\mathbf{x}}_0, \mathbf{z}_t)} - \frac{1}{f_t(\mathbf{x}, \mathbf{z}_t)} - \sum_{\mathbf{e} \neq \mathbf{z}_t} \frac{f_t(\mathbf{x}, \mathbf{e})}{f_t(\mathbf{x}, \mathbf{z}_t)} \log \frac{f_t(\tilde{\mathbf{x}}_0, \mathbf{z}_t)f_t(\mathbf{x}, \mathbf{e})}{f_t(\tilde{\mathbf{x}}_0, \mathbf{e})f_t(\mathbf{x}, \mathbf{z}_t)} \right) \quad (89)$$

Proof. since $k = 1, \mu = 0$, we have

$$\forall \mathbf{e}, r(\mathbf{e}) = r = \frac{1}{N} \quad (90)$$

hence

$$q(\mathbf{z}_s = \mathbf{e} | \mathbf{z}_t, \tilde{\mathbf{x}}_0) = \frac{f_s(\tilde{\mathbf{x}}_0, \mathbf{e})f_{t|s}(\mathbf{e}, \mathbf{z}_t)}{f_t(\tilde{\mathbf{x}}_0, \mathbf{z}_t)} \quad (91)$$

$$= \frac{(\alpha_s p_{\tilde{\mathbf{x}}_0, \mathbf{e}} + \beta_s/N)(\alpha_{t|s} p_{\mathbf{e}, \mathbf{z}_t} + \beta_{t|s}/N)}{\alpha_t p_{\tilde{\mathbf{x}}_0, \mathbf{z}_t} + \beta_t/N} \quad (92)$$

$$= \frac{N\alpha_t p_{\tilde{\mathbf{x}}_0, \mathbf{e}} \delta_{\mathbf{e}, \mathbf{z}_t} + \alpha_s \beta_{t|s} p_{\tilde{\mathbf{x}}_0, \mathbf{e}} + \alpha_{t|s} \beta_s \delta_{\mathbf{e}, \mathbf{z}_t} + \beta_s \beta_{t|s}/N}{N\alpha_t p_{\tilde{\mathbf{x}}_0, \mathbf{z}_t} + \beta_t} \quad (93)$$

$$= \frac{\delta_{\mathbf{e}, \mathbf{z}_t} (N\alpha_t p_{\tilde{\mathbf{x}}_0, \mathbf{e}} + \alpha_{t|s} \beta_s) + (\alpha_s - \alpha_t) p_{\tilde{\mathbf{x}}_0, \mathbf{e}} + \beta_s \beta_{t|s}/N}{N\alpha_t p_{\tilde{\mathbf{x}}_0, \mathbf{z}_t} + \beta_t} \quad (94)$$

given $s \rightarrow t$, for kl , we have

$$h_t(\mathbf{x}, \mathbf{z}_t) \quad (95)$$

$$= \frac{p_{\mathbf{x}, \mathbf{z}_t} - p_{\tilde{\mathbf{x}}_0, \mathbf{z}_t}}{f_t(\tilde{\mathbf{x}}_0, \mathbf{z}_t)} - \frac{1}{\alpha_t} \log \frac{f_t(\mathbf{x}, \mathbf{z}_t)}{f_t(\tilde{\mathbf{x}}_0, \mathbf{z}_t)} + \log \frac{f_t(\mathbf{x}, \mathbf{x})}{f_t(\tilde{\mathbf{x}}_0, \mathbf{x})} + \frac{k\beta_t}{N\alpha_t} \sum_{\mathbf{e}} \log \frac{f_t(\mathbf{x}, \mathbf{e})}{f_t(\tilde{\mathbf{x}}_0, \mathbf{e})} \quad (96)$$

$$= f_t(\mathbf{x}, \mathbf{z}_t) \frac{p_{\mathbf{x}, \mathbf{z}_t} - p_{\tilde{\mathbf{x}}_0, \mathbf{z}_t}}{f_t(\mathbf{x}, \mathbf{z}_t)f_t(\tilde{\mathbf{x}}_0, \mathbf{z}_t)} - \frac{1}{\alpha_t} \log \frac{f_t(\mathbf{x}, \mathbf{z}_t)}{f_t(\tilde{\mathbf{x}}_0, \mathbf{z}_t)} + \log \frac{f_t(\mathbf{x}, \mathbf{x})}{f_t(\tilde{\mathbf{x}}_0, \mathbf{x})} \quad (97)$$

$$+ \frac{\beta_t}{N\alpha_t} \sum_{\mathbf{e}} \log \frac{f_t(\tilde{\mathbf{x}}_0, \mathbf{z}_t)f_t(\mathbf{x}, \mathbf{e})}{f_t(\tilde{\mathbf{x}}_0, \mathbf{e})f_t(\mathbf{x}, \mathbf{z}_t)} - \frac{\beta_t}{N\alpha_t} \sum_{\mathbf{e}} \log \frac{f_t(\tilde{\mathbf{x}}_0, \mathbf{z}_t)}{f_t(\mathbf{x}, \mathbf{z}_t)} \quad (98)$$

$$= \frac{f_t(\mathbf{x}, \mathbf{z}_t)}{\alpha_t} \left(\frac{1}{f_t(\tilde{\mathbf{x}}_0, \mathbf{z}_t)} - \frac{1}{f_t(\mathbf{x}, \mathbf{z}_t)} \right) - \log \frac{f_t(\mathbf{x}, \mathbf{z}_t)}{f_t(\tilde{\mathbf{x}}_0, \mathbf{z}_t)} + \log \frac{f_t(\mathbf{x}, \mathbf{x})}{f_t(\tilde{\mathbf{x}}_0, \mathbf{x})} \quad (99)$$

$$+ \frac{\beta_t}{N\alpha_t} \sum_{\mathbf{e}} \log \frac{f_t(\tilde{\mathbf{x}}_0, \mathbf{z}_t)f_t(\mathbf{x}, \mathbf{e})}{f_t(\tilde{\mathbf{x}}_0, \mathbf{e})f_t(\mathbf{x}, \mathbf{z}_t)} \quad (100)$$

$$= \frac{f_t(\mathbf{x}, \mathbf{z}_t)}{\alpha_t} \left(\frac{1}{f_t(\tilde{\mathbf{x}}_0, \mathbf{z}_t)} - \frac{1}{f_t(\mathbf{x}, \mathbf{z}_t)} \right) - \log \frac{f_t(\mathbf{x}, \mathbf{z}_t)}{f_t(\tilde{\mathbf{x}}_0, \mathbf{z}_t)} + \log \frac{f_t(\mathbf{x}, \mathbf{x})}{f_t(\tilde{\mathbf{x}}_0, \mathbf{x})} \quad (101)$$

$$+ \frac{1}{\alpha_t} \sum_{\mathbf{e}} f_t(\mathbf{x}, \mathbf{e}) \log \frac{f_t(\tilde{\mathbf{x}}_0, \mathbf{z}_t)f_t(\mathbf{x}, \mathbf{e})}{f_t(\tilde{\mathbf{x}}_0, \mathbf{e})f_t(\mathbf{x}, \mathbf{z}_t)} - \log \frac{f_t(\tilde{\mathbf{x}}_0, \mathbf{z}_t)f_t(\mathbf{x}, \mathbf{x})}{f_t(\tilde{\mathbf{x}}_0, \mathbf{x})f_t(\mathbf{x}, \mathbf{z}_t)} \quad (102)$$

$$= \frac{f_t(\mathbf{x}, \mathbf{z}_t)}{\alpha_t} \left(\frac{1}{f_t(\tilde{\mathbf{x}}_0, \mathbf{z}_t)} - \frac{1}{f_t(\mathbf{x}, \mathbf{z}_t)} \right) + \frac{1}{\alpha_t} \sum_{\mathbf{e}} f_t(\mathbf{x}, \mathbf{e}) \log \frac{f_t(\tilde{\mathbf{x}}_0, \mathbf{z}_t)f_t(\mathbf{x}, \mathbf{e})}{f_t(\tilde{\mathbf{x}}_0, \mathbf{e})f_t(\mathbf{x}, \mathbf{z}_t)} \quad (103)$$

so

$$D_{KL} = \frac{\beta_{t|s}\alpha_s r(\mathbf{z}_t)}{f_t(\mathbf{x}, \mathbf{z}_t)} h_t(\mathbf{x}, \mathbf{z}_t) \quad (104)$$

$$= \frac{-\beta_{t|s}\alpha_s}{N\alpha_t} \left(\frac{1}{f_t(\mathbf{x}, \mathbf{z}_t)} - \frac{1}{f_t(\tilde{\mathbf{x}}_0, \mathbf{z}_t)} - \sum_{\mathbf{e}} \frac{f_t(\mathbf{x}, \mathbf{e})}{f_t(\mathbf{x}, \mathbf{z}_t)} \log \frac{f_t(\tilde{\mathbf{x}}_0, \mathbf{z}_t)f_t(\mathbf{x}, \mathbf{e})}{f_t(\tilde{\mathbf{x}}_0, \mathbf{e})f_t(\mathbf{x}, \mathbf{z}_t)} \right) \quad (105)$$

□

D. LM1B Sampling Case

We investigate the relationship between the inference computational budget (defined by the number of sampling steps T) and the perceptual quality of the generated text. Tab. 5 presents randomly selected, non-curated samples from the XDLM model trained on the LM1B. Each sample represents the final output of a distinct diffusion process constrained to a specific total step count $T \in \{4, 8, 16, 32, 64, 128\}$.

At the lower bound of the sampling budget ($T = 4$), the model fails to converge to the data manifold. the output is characterized by disjointed lexical retrieval (e.g., “*the advertising -tag prong*”) where individual tokens are valid but lack syntactic binding. Increasing the budget to $T = 8$ yields the emergence of superficial syntactic structures (e.g., “*curt schilling is a man of newness*”), yet the semantic content remains illogical, indicating that the diffusion process resolves local grammatical dependencies prior to higher-order semantic meaning.

As the sampling steps increase to the intermediate regime ($T = 16$ and $T = 32$), we observe a transition from mere grammatical correctness to narrative plausibility. At $T = 16$, the text exhibits valid sentence structures but suffers from tautological repetition and thematic drift (e.g., “*middle east in the middle east*”). By $T = 32$, the model generates cohesive clauses with clear subject-verb-object relationships, although the specific entities often remain synthetic or hallucinatory (e.g., “*mr poundhead*”). This suggests that while 32 steps are sufficient for the model to learn the structural rules of the language, the denoising process has not yet fully aligned the output with the specific factual distributions of the training corpus.

A distinct phase transition in sample quality is observed at $T = 64$, which appears to represent the saturation point for high-fidelity generation. At this stage, the model produces semantically robust text indistinguishable from natural news data, successfully handling complex entity lists (e.g., “*Congo, Benin, Ivory Coast*”) and domain-specific terminology (e.g., “*National Transportation Safety Board*”). Extending the process to $T = 128$ yields marginal improvements in long-range consistency and the precision of quantitative figures, but the perceptual gain over $T = 64$ is significantly smaller than the leap observed from $T = 32$. This trajectory indicates that while XDLM requires a minimum threshold of approximately 64 steps to resolve fine-grained semantic details, further increases in computational cost yield diminishing returns in generation quality.

Table 5. Uncurated samples generated by XDLM trained on LM1B. Each sample represents the output of a distinct diffusion process constrained to a specific total step count T . The sequence length is fixed at 128 tokens.

Steps (T)	Generated Text Sample
$T = 4$	[CLS]n. [CLS] the advertising -tag prong those former candidates is sept. [CLS] new and aspiring contenders boasted a present, confusing not candidates not only for 15 - u running bonds. [CLS] passengers on board the puerto rico jet jet out to the ash oftwa, hawaii, wednesday that afternoon. [CLS] as a result of the fusion going from in horsepower and to okter and the ram and to gm, s rentalearing / thirds was the infall. [CLS] times square may undergo restorations [CLS] and " old allah " is an homage to " the a, the " god " in snowy islamic faith. [CLS] unfortunately christina sees, [CLS]
$T = 8$	[CLS] be obese to go over. [CLS] curt schilling is a man of newness. [CLS] mr middle had, having not started the business for 15 years, wondered for one only anyone on board had once wanted from kraft. [CLS] the new oft - appointed owner proposed wednesday that the administration should take a " punitive tax supplement from treasury " and insisted on indiana and michigan adhering to gm's contract terms. [CLS] ms. cummings : one at times decides to undergo restoration. [CLS] and for now pakistani parliament is now resigned to a democratic, destabilization vote in parting zardari, which sees itself [CLS]

Steps (T)	Generated Text Sample (Continued)
$T = 16$	[CLS] " fails to clear advertising restrictions. [CLS] the network, which is the only known new middle east in the middle east, is expected for about 10 to 15 years. [CLS] i believe the people on board had called very pleased, how i was able to explain it in me. [CLS] the studio 86 is nearly a lot of contemporary televised - auto show - marquees - cars. the pre - gm bio tasted like two - thirds of iconic americans : one - third of the time that ford used and around 4 years the original was back to a building it made years of. [CLS] in contrast, zardari, who sees washington [CLS]
$T = 32$	[CLS] me, to clear the books. [CLS] that sense of neutrality is likely to force some postponements of the dispute, which was resolved wednesday. [CLS] 15 told the telegraph that he always believed the board had convinced him it was time to take the train. [CLS] mr poundhead wants the city council to create a series of new visitors' areas. [CLS] marfor, according to le monde, " is the afghans to steal or take and foot out " -- money the taliban has often used to buy from pakistani taliban, not pakistan's. [CLS] though some of its friends in the west zardari said he sees k [CLS]
$T = 64$	[CLS] me, was the crew of the xv230, which is carrying congo, benin, ivory coast, cape verde, manchester russians and coastguards at luanda. [CLS] the national transportation safety board had called the electrical life support vests to a safe spot above hawaii. [CLS] the daily herald said analysts expect earnings of \$ 394 million, or 43 cents a share, due to better - than - expected growth in the mini market. [CLS] general cuddy writes that the controls could be used to prevent revenge attacks, but not to halt the protests by those suspected of disturbing network in the island, throwing up the theory. [CLS] [CLS]
$T = 128$	[CLS] me to represent the cuban people they represent. [CLS] the leadership is still taking control of the company, but the problem has not been resolved. [CLS] to tony fernanda santos, of eey investments board, it thought up life's 328 million - and one - pound tax loss of \$ 86 million and projected earnings of \$ 37 million next year to 2011. [CLS] next up is " best of belies, " the first mini - series. [CLS] cusuoga, the nationalist method often used to describe revenge attacks, is not experienced in most protests against a presence of the tigers in the island's sinhala territories. [CLS] [CLS]

To investigate the internal generation mechanism of XDLM, we visualize a single generation trajectory with a total budget of $T = 32$ steps and a fixed sequence length of 128 tokens. Tab. 6 details the evolution of the sequence at steps $t \in \{0, 1, 8, 16, 24, 32\}$. We utilize a color-coded schema to distinguish the specific transition types inherent to the hybrid noise process. **Green** denotes transitions from the absorbing state ([MASK]) to a token (typical of Masked DLMs), **Blue** denotes token-to-token refinement (typical of Uniform DLMs), and **Red** denotes the re-masking operation (token back to [MASK]). This red transition is particular to XDLM, where the forward process is a mixture of absorbing and uniform noise, allowing the model to stochastically backtrack by rejecting previously generated tokens.

The process initializes at $t = 0$ with a mixture of masks and random tokens derived from uniform noise, such as "coffin," "slippery," and "trumpets." A critical dynamic is observed immediately at the transition to $t = 1$. The model actively rejects the majority of these random initializations. We observe extensive **Red** markings where tokens like "coffin" and "trumpets" are reverted to [MASK]. This demonstrates that XDLM is not strictly bound by its random initialization from the uniform noise. Unlike standard iterative refinement models that might struggle to escape local minima induced by poor random seeds, XDLM possesses the capacity to identify low-probability tokens and "clean the slate" via re-masking. Simultaneously, valid anchor tokens begin to emerge (**Green**), such as "shillings" and "blocked," establishing an initial semantic direction.

As the generation progresses through the intermediate steps ($t = 1 \rightarrow t = 16$), the model engages in a dynamic interplay of generation and error correction. The presence of all three transition types indicates a non-monotonic search process. The model generates new candidates (**Green**) and refines existing ones (**Blue**), but crucially, it continues to utilize re-masking (**Red**) to prune inconsistent branches. For instance, tokens generated tentatively in early steps are masked again when they

fail to align with the evolving global context.

By the final phase ($t = 24 \rightarrow t = 32$), the dynamics shift characteristically. The **Red** re-masking transitions disappear entirely, indicating structural convergence. The process focuses exclusively on filling remaining gaps (**Green**) and performing fine-grained lexical substitutions (**Blue**). Notable refinements occur here, such as the token “*life infancy*” at step 24 being refined to “*was time*” at step 32, and “*from pound*” refining to “*from pound-land*.” This trajectory confirms that XDLM successfully anneals from a high-temperature exploration state—characterized by active deletion and re-generation—to a low-temperature refinement state, ensuring the final output is both globally coherent and locally precise.

Table 6. Step-wise evolution of a generated sequence ($T = 32$). Text colors indicate the transition dynamics inherent to the hybrid noise process: **Green** represents new tokens generated from masks; **Blue** represents lexical refinement; and **Red** highlights the re-masking operation where previously generated tokens are rejected and reverted to `[MASK]`.

Steps (T)	Generated Text Sample
$T = 0$	[MASK] [MASK] faltered [MASK] [MASK] coffin [MASK] [MASK] [MASK] [MASK] och [MASK] slippery [MASK] [MASK] [MASK] [MASK] [MASK] [MASK] [MASK] [MASK] [MASK] [MASK] [MASK] [MASK] harrington [MASK] [MASK] [MASK] [MASK] [MASK] [MASK] [MASK] [MASK] [MASK] trumpets surpassing [MASK] refuse [MASK] [MASK] [MASK] [MASK] [MASK] [MASK] [MASK] ##was veteran jan [MASK] [MASK] [MASK] [MASK] [MASK] [MASK] [MASK] [MASK] [MASK] [MASK] [MASK] [MASK] [MASK] [MASK] [MASK] [MASK] begs [MASK] [MASK]
$T = 1$	[MASK] [MASK] faltered [MASK] [MASK] [MASK] [MASK] [MASK] [MASK] [MASK] [MASK] ##fo [MASK] is [MASK] [MASK] shillings [MASK] [MASK] [MASK] [MASK] [MASK] [MASK] [MASK] [MASK] [MASK] 1879 [MASK] [MASK] [MASK] [MASK] [MASK] ##anda [MASK] blocked [MASK] ##agawa [MASK] engined [MASK] [MASK] [MASK] a [MASK] [MASK] ##itive [MASK] [MASK] [MASK] [MASK] [MASK] mar [MASK] [MASK] [MASK] [MASK] [MASK] [MASK] [MASK] distributing [MASK] tertiary [MASK] [MASK] [MASK] [MASK] [MASK] [MASK] [MASK] [MASK] [MASK] strode [MASK] [MASK] [MASK] [MASK] [MASK] [MASK] [MASK] whatever [MASK] ##rda [MASK] [MASK] [MASK] [MASK] [MASK]
$T = 8$	[MASK] [MASK] [MASK] to clear [MASK] [MASK] [MASK] [CLS] [MASK] [MASK] of [MASK] is [MASK] congo [MASK] [MASK] [MASK] [MASK] [MASK] [MASK] ##rians santa , [MASK] [MASK] [MASK] [MASK] [MASK] [MASK] 15 [MASK] ##anda [MASK] [MASK] [MASK] [MASK] [MASK] board had [MASK] ##ffi [MASK] [MASK] [MASK] ##illo [MASK] the [MASK] [MASK] [CLS] [MASK] hawaii [MASK] [MASK] the [MASK] 86 to [MASK] a [MASK] of process [MASK] [MASK] [MASK] [MASK] [CLS] mar [MASK] [MASK] [MASK] [MASK] [MASK] , [MASK] [MASK] [MASK] [MASK] [MASK] [MASK] [MASK] [MASK] [MASK] [MASK] brazil [MASK] [MASK] [MASK] [MASK] [MASK] the [MASK] [MASK] [MASK] used [MASK] [MASK] [MASK] pakistani [MASK] [MASK] [MASK] [MASK] ' s [MASK] [MASK] ##west [MASK] [MASK] [MASK] [MASK] in [MASK] [MASK] za ##rda [MASK] [MASK] [MASK] sees [MASK] [MASK]

Steps (T)	Generated Text Sample (Continued)
$T = 16$	[MASK] [MASK] to clear [MASK] [MASK] [CLS] [MASK] [MASK] of [MASK] is [MASK] congo [MASK] [MASK] [MASK] [MASK] [MASK] the [MASK] , which [MASK] resolved obscene . [CLS] 15 [MASK] ##anda [MASK] [MASK] [MASK] [MASK] board had convinced ##ffi [MASK] life [MASK] [MASK] take the [MASK] [MASK] [CLS] [MASK] hawaii [MASK] [MASK] the city 86 to [MASK] a [MASK] of new [MASK] [MASK] areas [MASK] [CLS] mar [MASK] vice [MASK] [MASK] le [MASK], [MASK] [MASK] [MASK] afghan [MASK] to steal [MASK] [MASK] [MASK] out [MASK] - [MASK] [MASK] the taliban has often used to [MASK] from pakistani [MASK] [MASK] not pakistan 's [MASK] [MASK] though [MASK] of its [MASK] in [MASK] [MASK] za ##rda ##ri said [MASK] sees [MASK] [MASK]
$T = 24$	[MASK] [MASK] to clear [MASK] [MASK] . [CLS] that [MASK] of neutrality is [MASK] congo force some post ##pone ##ments of the [MASK], which [MASK] resolved [MASK] . [CLS] 15 [MASK] the telegraph that [MASK] [MASK] believed the board had convinced him [MASK] life infancy [MASK] take the train [MASK] [CLS] from pound [MASK], the city plans to [MASK] a [MASK] of new [MASK] [MASK] areas [MASK] [CLS] mar [MASK], according [MASK] le monde , " is the afghan ##s to steal or [MASK] and foot out " - - [MASK] the taliban has often used to [MASK] from pakistani taliban [MASK] not pakistan 's [MASK] [MASK] though [MASK] of its friends in the [MASK] za ##rda ##ri said he sees [MASK] [MASK]
$T = 32$	[CLS] me , to clear the flag . [CLS] that kind of neutrality is likely to force some post ##pone ##ments of the dispute , which was resolved wednesday . [CLS] 15 told the telegraph that he always believed the board had convinced him it was time to take the train . [CLS] from pound ## land , the city plans to build a series of new retail residential areas . [CLS] mar ## for , according to le monde , " is the afghan ##s to steal or take and foot out " - - money the taliban has often used to buy from pakistani taliban , not pakistan 's. [CLS] though some of its friends in the west za ##rda ##ri said he sees k [CLS]

E. ImageNet Sampling Case

We conduct a qualitative comparison of XDLM against the baseline models MDLM, GIDD, and UDLM on ImageNet-1K. The results are analyzed across two settings: unguided generation (Fig. 5) and generation with slight classifier-free guidance (Fig. 6). The visual evidence underscores XDLM’s unique ability to combine the strengths of absorbing and uniform noise strategies while mitigating their individual weaknesses.

The unguided setting serves as a stress test for structural priors. Here, the limitations of MDLM and GIDD are most apparent. These models struggle to form coherent geometries, resulting in chaotic texture blobs (e.g., the flamingo and ladybug columns) rather than distinct objects. Conversely, UDLM, which relies solely on uniform noise, successfully captures global shapes but fails to generate high-frequency details, resulting in blurry, out-of-focus images.

XDLM distinguishes itself by balancing these two extremes. By integrating the structural rigidity of MDLM with the refinement flexibility of UDLM, XDLM achieves structural coherence without sacrificing sharpness. For instance, in the rocket launch example, XDLM is the only model that renders a clear vertical fuselage and distinct smoke plumes without guidance.

As illustrated in Fig. 6, introducing a guidance scale of 2.0 improves general sample quality, yet the characteristic behaviors of the models persist. MDLM continues to suffer from lack of detail refinement, often producing over-saturated textures, with poor semantic structure. UDLM remains overly smooth; while the images are clean, they lack the crispness required for photorealism.

XDLM leverages the guidance most effectively to enhance detail. This is evident in the flock of flamingos. XDLM renders distinct, individual birds with sharp feathers, whereas MDLM merges them into a mass and UDLM blurs the boundaries. Similarly, in the food categories (strawberries and pizza), XDLM generates realistic surface textures and lighting reflections that are absent in the UDLM samples and distorted in the MDLM samples. This confirms that XDLM’s hybrid noise

mechanism provides a superior foundation for high-fidelity generation.



Figure 5. Qualitative comparison of class-conditional generation on ImageNet-1K without CFG. In the absence of guidance, baseline models struggle significantly: MDLM and GIDD produce chaotic artifacts with poor structural coherence, while UDLM yields recognizable but over-smoothed images. XDLM, by effectively balancing the characteristics of MDLM and UDLM, generates the most coherent and semantically correct samples (e.g., the distinct rocket structure and pizza toppings) even without guidance.



Figure 6. Qualitative comparison of class-conditional generation on ImageNet-1K with a CFG scale of 2.0. With the addition of guidance, all models improve, but quality disparities remain. MDLM and GIDD still exhibit texture distortion and "burn" artifacts. UDLM produces clean but blurry outputs, lacking fine-grained texture. XDLM demonstrates superior fidelity, combining sharp high-frequency details (seen in the strawberry and volcanoes) with accurate global structure.

We further analyze the sampling dynamics of XDLM ($k = 0.1$) over an 8-step generation process on ImageNet-1K with a CFG of 2.0, comparing it against MDLM, GIDD, and UDLM. The visual progression highlights distinct behaviors in how each model handles noise and feature refinement.

A critical advantage of XDLM is its strong refinement capability, facilitated by the integration of uniform noise throughout the sampling process. As observed in rows 3 and 4, both XDLM and UDLM begin generating key semantic features, specifically the dog's nose and eyes, at the very beginning of the generation cycle. In contrast, MDLM and GIDD adopt a

more conservative approach. They exhibit little to no refinement of these specific features. Consequently, by the final step [8/8], MDLM and GIDD still fail to resolve the proper structure of the nose and eyes, leaving them distorted or missing. XDLM, however, establishes these features early and refines them continuously, resulting in a anatomically correct and aesthetically pleasing final output.

The models also differ significantly in their ability to generate fine textures, such as the dog’s fur. Because MDLM lacks the ability to correct or refine previously generated tokens, the resulting fur texture appears rough and incoherent. While GIDD produces more delicate fur than MDLM, its performance is hindered by its reliance on time-variant noise, where the beneficial uniform noise mechanism only functions effectively during the very last step, limiting the potential for gradual improvement. Conversely, XDLM refines the fur texture consistently across all steps, ultimately producing the most realistic and high-fidelity texture among the group.

Last but not least, the comparison demonstrates that relying exclusively on uniform noise, as seen in UDLM, is insufficient for optimal image quality. While UDLM shares XDLM’s ability to locate features early, the final generated image is significantly more blurred. This lack of sharpness results in a loss of fine-grained details compared to XDLM, which successfully balances structural coherence with sharp, detailed textures.

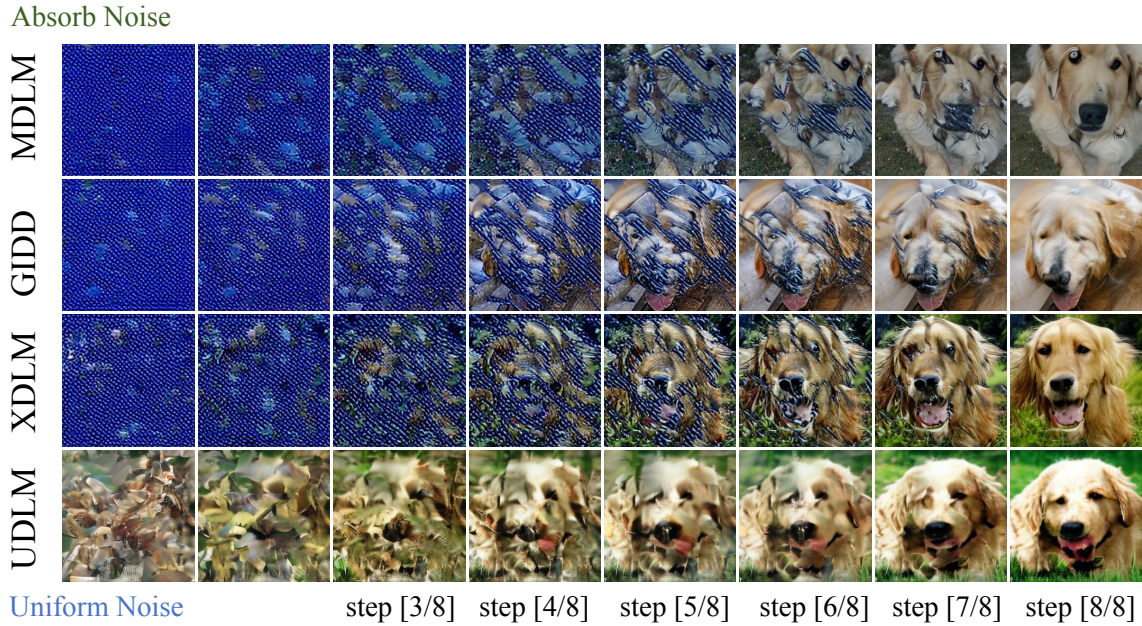


Figure 7. Visual comparison of sampling dynamics over 8 steps on ImageNet-1K. The figure contrasts the generation trajectories of MDLM, GIDD, XDLM ($k = 0.1$), and UDLM with CFG scale = 2.0. XDLM demonstrates superior structural coherence and detail refinement compared to baseline models, successfully transitioning from noise to a high-fidelity image.

F. Detailed Configurations of Experiments

Language Modeling Following established methodologies (Sahoo et al., 2025; Schiff et al., 2024; Sahoo et al., 2024), we evaluate our model on standard benchmarks using the LM1B (Chelba et al., 2013) and OpenWebText (OWT) (Gokaslan & Cohen, 2019) datasets. For LM1B, we detokenize the dataset following (Lou et al., 2023; Sahoo et al., 2024; 2025) and evaluate with (Austin et al., 2021; Sahoo et al., 2025) sequence packing. Sequences are processed with a context length of 128 using the bert-base-uncased tokenizer (Devlin et al., 2019). For OWT, we use the GPT-2 tokenizer (Radford et al., 2019) with a context length of 1,024. Sequences are packed to a maximum length of 1,024 with an EOS token delimiter. As OWT lacks a standard validation split, we reserve the last 100k documents for validation (Sahoo et al., 2024).

Consistent with prior work (Sahoo et al., 2024; Schiff et al., 2024; Sahoo et al., 2025), we parameterize both XDLM and baselines using the modified Diffusion Transformer (DiT) architecture (Peebles & Xie, 2023) adapted from (Lou et al., 2023). All models employ 12 layers, 12 attention heads, a hidden dimension of 768, and a timestep embedding dimension of

128. The dropout rate is set to 0.1, and input/output word embeddings are untied. To ensure fair comparison, we retain the AdaLN branch but fix the input to zero instead of using log-linear scheduled time embedding.

We train using AdamW ($\beta_1 = 0.9, \beta_2 = 0.999$, weight decay 0) with a global batch size of 512. The learning rate is warmed up to 3×10^{-4} over the first 2,500 steps and held constant thereafter. We apply an Exponential Moving Average (EMA) rate of 0.9999 (Sahoo et al., 2024; 2025).

Image Generation We evaluate on discretized CIFAR-10 (Krizhevsky et al., 2009) and ImageNet-1K (Deng et al., 2009).

On ImageNet-1K dataset, We use the VQ-VAE tokenizer from LlamaGen (Sun et al., 2024), , which compresses images into sequences of length 256. The backbone architecture mirrors our language modeling transformer, augmented with class-conditional embeddings to enable class-conditional generation. Training hyperparameters follow the language modeling configuration, with the training duration set to 0.5M steps.

For CIFAR-10, we treat raw RGB pixel values as discrete tokens (vocabulary size 256) and flatten the images into sequences of length $32 \times 32 \times 3$, following (Schiff et al., 2024). We employ a U-Net backbone (Ronneberger et al., 2015; Ho et al., 2020) with a discretized truncated logistic output distribution (Austin et al., 2021; Sahoo et al., 2024). Class conditioning is implemented by adding label embeddings to the timestep embeddings (Dhariwal & Nichol, 2021). The model is trained for 300k steps using AdamW ($\beta_1 = 0.9, \beta_2 = 0.999$, weight decay 0) with a batch size of 512. We use a learning rate warmup of 5,000 steps peaking at 2×10^{-4} and maintain an Exponential Moving Average (EMA) rate of 0.9999.

Large Language Model Tuning We scale XDLM to large language modeling by performing continual pretraining on LLaDA LLaDA (Nie et al., 2025), a model originally trained via MDLM. We utilize a 10-billion-token subset of the FineWeb-Edu dataset (Penedo et al., 2024). The training configuration employs a sequence length of 4,096 and a global batch size of 512. The learning rate is warmed up to 2×10^{-5} over 100 steps and held constant for the remaining 500 steps.

Unless otherwise specified, we set the mixing ratio to $k = 0.1$. All experiments were conducted on a node equipped with 8× Nvidia H800 GPUs.

G. Details of Zeroshot Capability of XDLM Trained on OWT

To comprehensively assess the generalization capabilities of XDLM, we evaluate zero-shot perplexity on seven external datasets following training on OWT. In this section, we provide the detailed experimental setup, an analysis of the hyperparameter sensitivity regarding the mixing ratio k , and a breakdown of the training dynamics.

Aligning with prior work (Sahoo et al., 2024; 2025), our evaluation suite includes the validation splits of AG News (Zhang et al., 2015), LAMBADA (Paperno et al., 2016), LM1B (Chelba et al., 2013), Penn Treebank (Marcus et al., 1993), Scientific Papers from ArXiv and PubMed (Cohan et al., 2018), and WikiText (Merity et al., 2016). The validation PPL is estimated via the negative Evidence Lower Bound (ELBO) with Monte Carlo sampling. We employ an evaluation batch size of 128 on a single GPU, and all text is pre-packed into a sequence length of 1024. To ensure a fair comparison, we adopt the identical sampling configuration used in(Sahoo et al., 2024; 2025).

We investigate the impact of the mixing ratio k on model performance. Tab. 7 and Tab. 8 present the validation PPL on OWT and the zero-shot PPL on external benchmarks, respectively.

As shown in Tab. 7, XDLM exhibits performance highly correlated with k . With smaller values (e.g., $k = 1e-3$ and $k = 0.1$), XDLM achieves a PPL of 23.495 and 24.097, respectively, which is comparable to MDLM (23.321) and GIDD (23.136). Conversely, as k increases towards 0.9, the performance degrades to 25.731, approaching the UDLM baseline (25.937).

This trend is further supported by the zero-shot benchmark results in Tab. 8. XDLM ($k = 0.1$) achieves an average PPL of 54.110, performing similarly to MDLM (53.650) and significantly outperforming UDLM (59.574). This demonstrates that XDLM successfully retains the strong modeling capabilities of the masked diffusion paradigm.

Notably, the superior performance of XDLM is not merely an endpoint phenomenon but a consistent property observed throughout the training process. As illustrated in Fig. 8, the PPL trajectory of XDLM closely aligns with that of MDLM, steadily decreasing from 64.85 to 54.11. In contrast, the UDLM curve remains notably higher across all training steps. Tab. 9 details the average zero-shot PPL at 100k step intervals. The data confirms that XDLM ($k = 0.1$) maintains a learning dynamic nearly identical to MDLM from the early stages (100k steps) to convergence (1M steps), highlighting the inherent

stability and efficiency of the proposed method.

Table 7. Validation PPL on OWT after 1M training steps. Performance is highly correlated with the mixing ratio k : lower values ($k \leq 0.1$) maintain parity with the strong MDLM baseline (23.321), while higher values ($k \rightarrow 0.9$) degrade towards the UDLM baseline (25.937).

Model	MDLM	GIDD	XDLM($k=1e-3$)	XDLM($k=0.1$)	XDLM($k=0.5$)	XDLM($k=0.9$)	UDLM
PPL	23.321	23.136	23.495	24.097	24.818	25.731	25.937

Table 8. Zero-shot PPL evaluation on seven external benchmarks. XDLM ($k = 0.1$) demonstrates robust generalization, achieving an average PPL (54.110) comparable to pure mask-based methods (MDLM/GIDD) and significantly outperforming UDLM (59.574).

Dataset	AG News	LAMBADA	LM1B-GPT2	PTB	ArXiv	PubMed	WikiText	Average
MDLM	61.374	47.967	65.629	89.049	37.457	41.981	32.093	53.650
GIDD	60.607	47.811	65.898	86.911	39.019	42.634	30.809	53.384
XDLM($k=1e-3$)	62.247	45.982	65.944	89.575	38.294	42.206	31.809	53.722
XDLM($k=0.1$)	62.768	45.608	68.229	90.796	37.232	41.391	32.748	54.110
XDLM($k=0.5$)	67.352	47.966	71.252	91.683	38.460	43.373	33.570	56.236
XDLM($k=0.9$)	71.791	49.094	74.116	97.266	39.658	44.701	35.175	58.829
UDLM	69.402	51.272	75.572	95.986	42.671	47.181	34.933	59.574

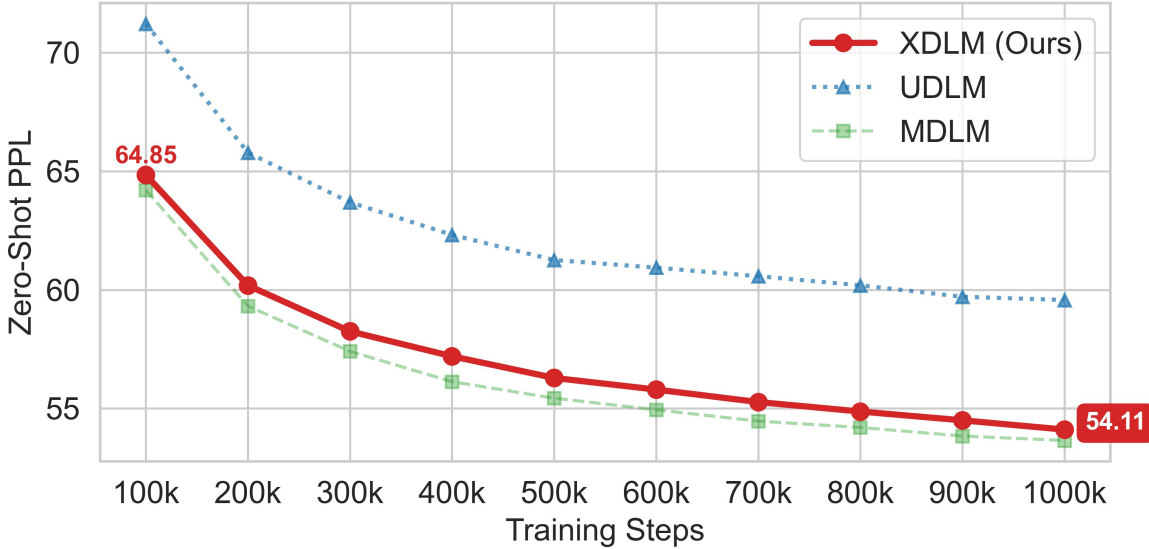


Figure 8. Average Zero-Shot PPL trajectory throughout training. Consistent with the final results, XDLM ($k = 0.1$) closely aligns with the MDLM baseline from early stages (64.85) to convergence (54.11), while the UDLM curve remains notably higher across all training steps.

Table 9. Detailed evolution of Zero-Shot PPL throughout training. Evaluated at 100k-step intervals, the data confirms that XDLM ($k = 0.1$) maintains a learning dynamic nearly identical to MDLM, highlighting the method’s stability and efficiency from early training to convergence.

Train Steps	100k	200k	300k	400k	500k	600k	700k	800k	900k	1M
MDLM	64.209	59.315	57.411	56.129	55.434	54.943	54.466	54.201	53.839	53.650
GIDD	61.097	57.900	56.326	55.389	54.848	54.294	53.960	53.807	53.258	53.384
XDLM($k=1e-3$)	63.748	59.097	57.319	56.374	55.576	54.937	54.577	54.336	53.977	53.722
XDLM($k=0.1$)	64.847	60.187	58.253	57.201	56.288	55.797	55.271	54.872	54.500	54.110
XDLM($k=0.5$)	68.074	62.524	60.489	59.353	58.396	57.881	57.437	56.976	56.530	56.236
XDLM($k=0.9$)	70.264	65.384	63.147	61.758	60.977	60.263	59.723	59.438	58.915	58.829
UDLM	71.220	65.789	63.692	62.320	61.258	60.937	60.577	60.192	59.711	59.574

H. Detailed Language Generation Results

In this section, we present the comprehensive numerical results for the language generation experiments initially discussed in Sec. 4.2. To systematically analyze the trade-off between the absorbing (MDLM-like) and uniform (UDLM-like) diffusion processes, we evaluate XDLM across varying mixing ratios $k \in \{10^{-3}, 0.1, 0.5, 0.9\}$. For generation, we adopt the *ancestral* sampling setting (Sahoo et al., 2024; Schiff et al., 2024; Sahoo et al., 2025), employing parallel token sampling from the estimated posterior via Gumbel noise. The resulting performance is evaluated based on sample quality, quantified by GPT-2 Large perplexity (PPL \downarrow), and diversity, measured by Token Entropy (\uparrow).

Tab. 10 presents the comprehensive evaluation on the OWT dataset. The data quantitatively confirms that k governs the model’s performance across different numbers of sampling steps, effectively interpolating between the behaviors of UDLM and MDLM. In the few-step regime (e.g., 8 to 32 sampling steps), increasing k significantly improves performance, aligning XDLM with the efficiency of UDLM. For instance, with only 8 sampling steps, XDLM ($k = 0.9$) yields a low perplexity of 189.750, which is highly competitive with UDLM (183.991) and vastly superior to the mask-based baselines, MDLM (711.382) and GIDD (654.841). Conversely, in the multi-step regime (e.g., 512 to 1024 sampling steps), retaining mask-like properties (lower k) remains advantageous for achieving high-fidelity generation. XDLM ($k = 0.1$) demonstrates an optimal balance. It dramatically improves upon MDLM when sampling budget are limited, while retaining the capacity to reach very low perplexity scores (52.609 at 1024 steps) when more sampling steps are available, all without sacrificing the diversity indicated by entropy.

These findings are corroborated by the results on the LM1B dataset, detailed in Tab. 11. We observe a consistent trend where a higher k dominates when the number of sampling steps is small. At 4 sampling steps, XDLM ($k = 0.5$) achieves a perplexity of 232.702, effectively matching UDLM (232.403) and significantly outperforming MDLM (377.177). As the number of sampling steps increases, the performance gaps narrow, yet XDLM remains robust across the spectrum. Collectively, these results demonstrate that by tuning k , XDLM bridges the gap between the two paradigms: it captures the efficiency of uniform noise at few sampling steps while preserving the high-quality potential of masking at larger steps.

Table 10. Quality (PPL) vs. Diversity (Entropy) on OWT. The results demonstrate that the optimal mixing ratio k depends on the sampling budget. In the few-step regime (e.g., 8 steps), a higher k is essential for efficiency, allowing XDLM to match UDLM performance. Conversely, in the multi-step regime, a lower k becomes advantageous for achieving high fidelity. Notably, XDLM ($k = 0.1$) strikes an optimal balance, dramatically outperforming MDLM at low step counts while reaching superior perplexity at high step counts.

Model	step 8	step 16	step 32	step 64	step 128	step 256	step 512	step 1024
<i>Perplexity ↓</i>								
MDLM	711.382	288.157	156.576	106.098	80.198	64.376	51.756	41.545
GIDD	654.841	273.829	151.331	102.558	77.548	62.077	49.822	39.981
XDLM($k=1e-3$)	613.647	253.897	146.567	104.090	80.301	65.245	52.650	42.797
XDLM($k=0.1$)	301.640	161.724	114.795	94.837	83.205	73.824	63.888	52.609
XDLM($k=0.5$)	218.572	127.335	98.817	86.956	81.051	77.155	73.503	66.136
XDLM($k=0.9$)	189.750	117.234	93.239	84.068	80.614	79.456	78.707	78.238
UDLM	183.991	111.237	88.632	79.509	76.611	74.019	73.345	106.666
<i>Entropy ↑</i>								
MDLM	5.872	5.767	5.687	5.614	5.543	5.472	5.387	5.287
GIDD	5.832	5.748	5.675	5.605	5.534	5.462	5.370	5.269
XDLM($k=1e-3$)	5.837	5.746	5.673	5.613	5.546	5.475	5.393	5.298
XDLM($k=0.1$)	5.662	5.630	5.600	5.573	5.548	5.516	5.467	5.390
XDLM($k=0.5$)	5.574	5.565	5.555	5.547	5.538	5.525	5.514	5.476
XDLM($k=0.9$)	5.546	5.547	5.548	5.548	5.548	5.547	5.544	5.542
UDLM	5.536	5.539	5.543	5.535	5.536	5.531	5.524	5.769

Table 11. Quality (PPL) vs. Diversity (Entropy) on LM1B. Corroborating the OWT findings, a higher k proves dominant when the sampling budget is strictly limited. At 4 steps, XDLM ($k = 0.5$) effectively matches UDLM. Across the full spectrum of sampling steps, XDLM bridges the gap between paradigms, capturing the efficiency of uniform noise for small budgets while preserving the high-quality potential of masking for larger budgets.

Model	step 4	step 8	step 16	step 32	step 64	step 128
<i>Perplexity ↓</i>						
MDLM	377.177	215.579	152.939	124.731	112.049	102.142
GIDD	392.002	215.873	151.824	124.014	110.247	101.211
XDLM($k=1e-3$)	343.246	199.457	146.612	124.444	111.960	103.544
XDLM($k=0.1$)	246.134	155.487	123.129	113.006	105.509	101.983
XDLM($k=0.5$)	232.702	141.121	116.063	106.182	103.419	100.754
UDLM	232.403	136.914	110.575	102.072	98.571	96.385
<i>Entropy ↑</i>						
MDLM	4.405	4.379	4.366	4.357	4.353	4.347
GIDD	4.401	4.373	4.361	4.359	4.354	4.348
XDLM($k=1e-3$)	4.382	4.363	4.357	4.358	4.354	4.351
XDLM($k=0.1$)	4.326	4.329	4.334	4.342	4.345	4.346
XDLM($k=0.5$)	4.309	4.315	4.325	4.335	4.340	4.342
UDLM	4.303	4.305	4.320	4.327	4.334	4.336

I. Detailed Image Generation Results

We present an extended analysis of XDLM’s image generation capabilities on ImageNet-1K and CIFAR-10, specifically examining the impact of the mixing ratio parameter k . As defined in our methodology, k governs the balance between the mask-based and uniform-noise processes. A higher k increases the proportion of uniform noise (effectively approaching the UDLM setting), while a lower k retains more mask-like properties. The results in Tab. 12, 13, 14, 15 empirically validate the utility of this interpolation. We observe two key behaviors: first, a consistent convergence of XDLM towards

UDLM behavior as k increases; and second, the fact that the optimal performance often lies within the interpolated regime ($0 < k < 1$) rather than at the extremes (pure MDLM or UDLM).

Tab. 12 and 13 detail the performance on ImageNet-1K, providing compelling evidence that the optimal k varies depending on the generation setting. In the standard conditioning regime (Tab. 12), a balanced mix is preferred: XDLM with $k = 0.5$ achieves an FID of 23.417 at 16 steps, significantly outperforming both the low-mixing variant ($k = 10^{-3}$) and the specialized UDLM baseline (26.242). However, when Classifier-Free Guidance (CFG) is applied (Tab. 13), the optimal operating point shifts. Here, $k = 0.1$ emerges as the “sweet spot,” achieving an FID of 8.625, which surpasses both the pure UDLM (8.980) and the $k = 0.5$ variant (8.790). These findings highlight the advantage of XDLM. By exploring the interpolation space between masking and uniform noise, we can identify configurations that outperform both individual baselines.

Tab. 14 and 15 further illustrate the behavioral shift controlled by k on CIFAR-10. On this benchmark, where UDLM demonstrates a distinct advantage, we observe a clear monotonic improvement in generation quality as k rises. For instance, under standard conditioning, increasing k from 10^{-3} to 0.5 improves the 32-step FID from 164.040 to 56.299, dramatically closing the gap with UDLM (41.027). A similar trend holds with CFG, where $k = 0.5$ approaches the UDLM benchmark. Collectively, these results confirm that XDLM successfully bridges the gap between domains. Crucially, it demonstrates that there is no single fixed k that is optimal for all scenarios; instead, the flexibility to tune k within the interval (0, 1) is essential for maximizing performance across different datasets and guidance regimes.

Table 12. Comparison of FID (↓) and IS (↑) on ImageNet-1K. For image generation, XDLM proves to be a very strong contender, achieving performance highly comparable to the specialized UDLM model. Notably, XDLM outperforms all baselines, including UDLM, at 16 generation steps, confirming its robust performance beyond the text domain.

Model	FID↓				IS↑			
	step 4	step 8	step 16	step 32	step 4	step 8	step 16	step 32
MDLM	80.752	47.732	28.785	18.928	16.287	29.178	44.656	57.803
GIDD	86.842	54.933	35.403	24.588	14.559	24.297	35.698	46.376
XDLM($k=1e-3$)	81.992	52.590	35.046	25.637	15.597	24.813	35.097	44.032
XDLM($k=0.1$)	54.085	34.109	25.774	22.187	24.829	36.964	43.903	48.118
XDLM($k=0.5$)	45.808	29.362	23.417	21.486	29.310	40.482	46.620	48.911
UDLM	49.861	30.144	26.242	25.661	27.049	38.832	41.801	41.850

Table 13. Performance on ImageNet-1K with CFG (scale = 2.0). The application of guidance shifts the optimal operating point. Here, $k = 0.1$ emerges as the “sweet spot,” achieving an FID of 8.625 at 16 steps. This configuration surpasses both the pure UDLM baseline (8.980) and the higher-mixing variant ($k = 0.5$), demonstrating the importance of tuning k for specific guidance regimes.

Model	FID↓				IS↑			
	step 4	step 8	step 16	step 32	step 4	step 8	step 16	step 32
MDLM	33.468	11.144	6.725	7.485	54.740	119.150	172.664	203.722
GIDD	41.000	15.151	7.076	6.314	44.084	95.789	148.148	181.017
XDLM($k=1e-3$)	32.876	12.872	7.612	7.588	53.351	102.601	144.019	167.660
XDLM($k=0.1$)	13.550	8.956	8.625	8.914	107.403	148.723	165.916	171.046
XDLM($k=0.5$)	11.945	9.038	8.790	8.939	114.135	145.718	156.339	159.829
UDLM	14.055	9.718	8.980	8.650	97.859	123.582	132.099	132.108

Table 14. Class-conditional generation on CIFAR-10. On this benchmark, where UDLM holds a distinct advantage, we observe a clear monotonic improvement in XDLM quality as k increases. Increasing k from 10^{-3} to 0.5 dramatically closes the performance gap with UDLM (e.g., improving 32-step FID from 164.040 to 56.299), confirming that higher k effectively aligns XDLM with uniform noise dynamics.

Model	FID \downarrow			IS \uparrow		
	step 32	step 128	step 512	step 32	step 128	step 512
MDLM	211.983	69.151	33.961	2.685	5.615	6.801
GIDD	193.487	72.579	41.809	2.737	5.176	6.209
XDLM($k=1e-3$)	164.040	50.638	29.079	3.427	6.223	7.079
XDLM($k=0.1$)	77.985	48.702	43.210	5.316	6.284	6.513
XDLM($k=0.5$)	56.299	37.307	33.030	6.077	6.801	6.956
UDLM	41.027	27.822	25.144	6.892	7.345	7.372

Table 15. Performance of XDLM and baselines on image generation with CFG scale = 2.0 on CIFAR-10. All mask-based methods (MDLM, GIDD, XDLM) show significant improvement when CFG is applied. The basic trend follows the results with no cfg.

Model	FID \downarrow			IS \uparrow		
	step 32	step 128	step 512	step 32	step 128	step 512
MDLM	181.453	51.113	22.762	3.329	6.969	8.078
GIDD	179.916	60.443	30.812	3.054	6.124	7.216
XDLM($k=1e-3$)	130.106	35.980	19.877	4.559	7.575	8.186
XDLM($k=0.1$)	59.600	36.889	32.444	6.699	7.596	7.670
XDLM($k=0.5$)	40.850	27.445	24.445	7.560	7.881	7.893
UDLM	30.328	20.720	18.592	8.098	8.392	8.433

J. Detailed LLaDA Continual Pretraining Results

To empirically validate the efficacy of the XDLM objective within the LLaDA framework, we conducted a continual pre-training experiment utilizing the LLaDA 8B Base checkpoints. We integrated the XDLM modeling definitions into the transformers codebase and trained on a 10 billion token sample of the FineWeb-Edu dataset (Penedo et al., 2024). The training process spanned 600 steps with a global batch size of 512 and a sequence length of 4,096. The learning rate was warmed up to 2×10^{-5} over the first 100 steps and held constant for the subsequent 500 steps, with the XDLM mixing ratio set to 0.1. All experiments were conducted on a compute node equipped with 8 \times Nvidia H800 GPUs. To rigorously attribute performance gains to the architectural paradigm rather than confounding variables, we established two robust baselines: LLaDA-MDLM, a control condition where the model is continual pre-trained for the same duration using the standard Masked Diffusion Language Model objective; and LLaDA-XDLM-infer, an ablation where the XDLM sampling strategy is applied to the base model without further training.

To deploy XDLM sampling within this architecture, we extended the standard low-confidence remasking strategy used in LLaDA. Algorithm 1 details the generation logic, highlighting the novel contributions in the conditional block controlled by the mixing ratio k . While standard LLaDA sampling operates via a monotonic reduction of uncertainty, prioritizing only the filling of existing [MASK] tokens, our implementation introduces a *refinement branch*. When $k > 0.0$, the algorithm calculates a ‘refine_priority’ by identifying tokens that are currently unmasked (‘is_masked’) but for which the model predicts a conflicting token ID (‘pred_tokens != token_ids’) with a confidence score exceeding the current token’s confidence. These tokens are flagged in ‘update_mask’ alongside the standard empty masks. This mechanism fundamentally transforms the generation from a purely additive process into a dynamic error-correction loop, allowing the model to stochastically “change its mind” and revise previous outputs during the denoising trajectory.

The empirical results, summarized in Tab. 16, demonstrate the superiority of this formulation across reasoning (GSM8K, MATH, BBH) and code generation (HumanEval, MBPP) benchmarks, particularly in low-compute regimes. At 32 sampling steps, LLaDA-XDLM significantly outperforms all baselines. The most distinct advantage is observed in the MBPP code generation task, where LLaDA-XDLM achieves a score of 15.00, effectively doubling the performance of the base LLaDA (6.80) and the continued MDLM control (4.40). A granular analysis of the MBPP failure modes reveals that this improvement

is driven by a fundamental enhancement in generative fidelity; LLaDA-XDLM drastically reduces the incidence of “Failed” cases, defined as non-compilable or syntactically invalid code, from 429 (LLaDA) to 304. By successfully converting these previously unproductive attempts into “Passed” outputs (75 vs. 34), the model confirms that the XDLM objective, combined with the refinement sampling strategy, provides the necessary structural coherence to self-correct syntactic errors that would otherwise lead to compilation failures. As sampling steps increase to 64, 128, and 256 (the total generation length), LLaDA-XDLM maintains a competitive edge, validating that the performance gains stem directly from the internal representation learned during XDLM training rather than being an artifact of the sampling algorithm alone.

Notably, we observe that the continual pretraining baseline (LLaDA-MDLM) exhibits a performance decline compared to the original LLaDA, likely due to the distribution shift between the tuning data and the original pretraining corpus. Consequently, the superior performance of LLaDA-XDLM over LLaDA-MDLM confirms that our gains stem from the effectiveness of the XDLM formulation rather than merely the additional 600 training steps.

Furthermore, LLaDA-XDLM significantly outperforms the ablation baseline LLaDA-XDLM-infer, demonstrating that the improvement is intrinsic to the learned model rather than being an artifact of sampling tricks.

Algorithm 1 Generation Strategy of LLaDA-XDLM

```

def generate(steps, seq_length, mask_id, topk_absorb, topk_uniform, k=0.1):
    """
    Args:
        steps (int): Total number of sampling steps.
        seq_length (int): Target sequence length to generate.
        mask_id (int): Vocabulary index of the [MASK] token.
        topk_absorb (list[int]): Schedule for the number of tokens to decode at each step.
        topk_uniform (list[int]): Schedule for the number of tokens to refine at each step.
        k (float): The mixing ratio.
    Returns:
        token_ids (torch.Tensor): The generated sequence of token IDs with shape (seq_length,).
    """
    token_ids = torch.full((seq_length,), fill_value=mask_id, dtype=torch.long)
    for i in range(steps):
        is_masked = (token_ids == mask_id)
        logits = model(token_ids).logits
        logits_with_noise = add_gumbel_noise(logits)
        pred_tokens = torch.argmax(logits_with_noise, dim=-1)
        probs = torch.softmax(logits, dim=-1)
        pred_confidence = torch.squeeze(torch.gather(probs, dim=-1, index=torch.unsqueeze(pred_tokens, -1)), -1)
        mask_priority = torch.where(is_masked, pred_confidence, -np.inf)

        if k > 0.0:
            current_confidence = torch.squeeze(torch.gather(probs, dim=-1, index=torch.unsqueeze(token_ids, -1)), -1)
            can_be_refined = (~is_masked) & (pred_tokens != token_ids) & (pred_confidence >= current_confidence)
            refine_priority = torch.where(can_be_refined, pred_confidence, -np.inf)

        update_mask = torch.zeros_like(pred_tokens, dtype=torch.bool)
        _, top_mask_indices = torch.topk(mask_priority, k=topk_absorb[i])
        update_mask[top_mask_indices] = True

        if k > 0.0:
            _, top_refine_indices = torch.topk(refine_priority, k=topk_uniform[i])
            update_mask[top_refine_indices] = True

        token_ids[update_mask] = pred_tokens[update_mask]

    return token_ids

```

Table 16. Evaluation of LLaDA-XDLM on reasoning and code generation benchmarks. We compare the proposed method with the base LLaDA, an inference-only ablation (LLaDA-XDLM-infer), and an MDLM control (LLaDA-MDLM) across varying sampling steps. MBPP scores are decomposed into failure modes to illustrate structural correctness.

Dataset	BBH	GSM8K	MATH	HumanEval	MBPP			
					Score	Failed	Wrong	Pass
32 steps / 256 tokens								
LLaDA	42.68	24.49	4.80	5.49	6.80	429	37	34
LLaDA-XDLM-infer	41.74	24.26	4.86	1.22	5.40	438	35	27
LLaDA-MDLM	43.21	24.41	2.70	6.71	4.40	447	31	22
LLaDA-XDLM	42.76	29.26	4.72	10.98	15.00	304	121	75
64 steps / 256 tokens								
LLaDA	47.16	57.16	16.10	12.80	17.80	328	83	89
LLaDA-XDLM-infer	46.76	53.75	16.12	4.88	17.60	328	84	88
LLaDA-MDLM	48.32	54.97	13.42	14.63	13.40	348	84	67
LLaDA-XDLM	45.61	57.85	16.48	15.85	23.60	197	182	118
128 steps / 256 tokens								
LLaDA	47.49	67.93	26.12	24.39	27.60	161	199	138
LLaDA-XDLM-infer	47.89	66.41	26.70	8.54	27.40	187	174	137
LLaDA-MDLM	48.95	68.61	24.34	25.00	30.00	169	178	150
LLaDA-XDLM	46.41	68.01	25.06	25.00	30.80	130	215	154
256 steps / 256 tokens								
LLaDA	47.77	72.25	29.98	33.54	40.40	48	248	202
LLaDA-XDLM-infer	47.93	71.34	29.34	6.71	37.00	74	238	185
LLaDA-MDLM	49.84	72.93	29.70	32.32	37.60	51	260	188
LLaDA-XDLM	46.07	73.16	29.22	31.71	34.60	90	236	173

K. Detailed Computational Efficiency Analysis

We evaluate the computational efficiency of the proposed XDLM against baseline models by measuring speed and memory consumption across three distinct scenarios: the *forward-only* case (representing NELBO calculation for perplexity estimation), the *forward-backward* case (used in training), and the *sampling* case (used for generation). For the forward and forward-backward evaluations, we utilize randomly generated sequences with a batch size of 32 and a sequence length of 1024 to simulate real data processing. To ensure robust measurements, models are warmed up for 10 iterations, and we report the mean value calculated over the subsequent 100 runs. For the sampling scenario, we employ standard ancestral sampling to generate sequences of length 1024 over 32 steps. The evaluation batch size is set to 32. Models are warmed up for 1 iteration, and we report the mean value calculated over the subsequent 10 runs.

As detailed in Tab. 17, MDLM exhibits the highest throughput and lowest memory cost across all settings, a result expected due to the simplicity of its absorbing noise kernel. However, among models incorporating uniform noise distributions, XDLM achieves the highest throughput across the *forward*, *forward-backward*, and *sampling* regimes. This performance is directly attributed to our scalar reformulated efficient sampling and training strategy, which circumvents expensive matrix operations. In contrast, while UDLM maintains the third-highest throughput in forward and training modes, its sampling throughput is the lowest among the comparison group. Conversely, GIDD achieves the third-highest sampling throughput but performs poorly in NELBO calculation, reaching only half the forward throughput of XDLM. This trend is mirrored in memory consumption. While MDLM is the most lightweight overall, XDLM ranks first among methods whose noise kernel includes a uniform noise component, effectively avoiding the high memory overhead observed in GIDD and UDLM.

Table 17. Computational Efficiency Comparison. We report throughput (tokens/s, \uparrow) and peak memory usage (GB, \downarrow) for MDLM, GIDD, XDLM, and UDLM. The metrics cover three scenarios: *forward* (inference/perplexity estimation), *forward-backward* (training), and *sample* (generation). Leveraging the scalar reformulated strategy, XDLM achieves highly competitive throughput and memory efficiency, outperforming other baselines incorporating uniform noise kernels (GIDD, UDLM) in most metrics.

Model	Throughput (token/s) \uparrow			Memory (GB) \downarrow		
	forward	forward-backward	sample	forward	forward-backward	sample
MDLM	424294	141990	8789	6.285	35.354	18.848
GIDD	199516	95395	6336	25.131	51.060	40.856
XDLM (k=0.1)	396398	137372	7108	18.850	41.634	31.414
UDLM	370952	142276	2882	18.850	44.777	59.683

L. Detailed Training Dynamics

In this section, we provide the comprehensive numerical data corresponding to the training dynamics analysis discussed in Sec. 4.3 and visualized in Fig. 4. These tables supplement the visual analysis by providing exact metric values for Perplexity, Entropy, FID, and IS across the training trajectory.

Tab. 18 details the training dynamics on the LM1B benchmark over the course of 1 million training steps. The models were evaluated using a fixed budget of 128 sampling steps. As indicated in the main text, while MDLM exhibits superior performance in the initial phase, UDLM demonstrates strong scaling in later training stages, achieving the lowest perplexity among baselines by 1M steps (96.385). Furthermore, the table details the impact of varying the mixing ratio k within our proposed XDLM method.

Complementing the text generation results, Tab. 19 presents the quantitative training dynamics for image generation on ImageNet-1K. Evaluations were conducted over 500k training steps using a fixed budget of 16 sampling steps. The numerical data corroborates the visual trends: XDLM establishes and maintains a decisive performance advantage. Notably, XDLM with $k = 0.5$ achieves the lowest reported FID of 23.417 and the highest IS of 46.620 at the final checkpoint, consistently outperforming the MDLM and GIDD baselines. While UDLM starts with a higher FID, it converges rapidly to a competitive score (26.242), yet XDLM remains the leading model throughout the majority of the training phases.

Table 18. Quantitative training dynamics on the LM1B benchmark, supplementing the visual analysis in Fig. 4. We report Perplexity (\downarrow) and Entropy (\uparrow) over 1M training steps, utilizing a fixed budget of 128 sampling steps. The table details the impact of varying the mixing ratio k in XDLM compared to MDLM, GIDD, and UDLM baselines.

Train Steps	100k	200k	300k	400k	500k	600k	700k	800k	900k	1M
Perplexity \downarrow										
MDLM	113.218	107.864	106.735	105.839	104.594	104.106	103.559	103.174	102.769	102.142
GIDD	107.366	103.473	103.386	101.854	102.367	101.745	101.904	101.957	101.490	101.211
XDLM(k=1e-3)	112.628	108.381	106.406	104.913	105.156	103.817	103.624	102.731	103.638	103.544
XDLM(k=0.1)	119.632	110.803	109.017	106.265	105.428	104.572	103.645	103.348	102.223	101.983
XDLM(k=0.5)	117.846	111.024	108.130	105.955	104.953	103.048	102.464	101.040	102.015	100.754
UDLM	116.021	107.800	104.508	102.466	101.480	99.958	99.660	98.147	97.503	96.385
Entropy \uparrow										
MDLM	4.350	4.348	4.350	4.347	4.349	4.349	4.348	4.349	4.349	4.347
GIDD	4.352	4.350	4.351	4.349	4.351	4.349	4.350	4.350	4.351	4.348
XDLM(k=1e-3)	4.351	4.347	4.349	4.347	4.350	4.347	4.347	4.349	4.351	4.351
XDLM(k=0.1)	4.353	4.347	4.347	4.344	4.344	4.344	4.346	4.344	4.344	4.346
XDLM(k=0.5)	4.350	4.346	4.345	4.344	4.342	4.343	4.342	4.343	4.344	4.342
UDLM	4.349	4.343	4.341	4.340	4.338	4.336	4.338	4.336	4.335	4.336

Table 19. Quantitative training dynamics on ImageNet-1K generation, corresponding to the curves in Fig. 4. We report FID (↓) and IS (↑) over 500k training steps, utilizing a fixed budget of 16 sampling steps. The numerical data corroborates the visual trends: XDLM establishes and maintains a decisive performance advantage.

Train Steps	FID↓					IS↑				
	100k	200k	300k	400k	500k	100k	200k	300k	400k	500k
MDLM	40.060	33.723	31.090	29.436	28.785	28.978	36.136	39.804	42.893	44.656
GIDD	42.152	36.878	35.200	35.677	35.403	27.337	33.042	35.544	35.173	35.698
XDLM($k=1e-3$)	45.381	38.967	36.061	36.287	35.046	24.967	30.512	33.948	34.031	35.097
XDLM($k=0.1$)	38.358	31.464	27.524	26.853	25.774	27.949	35.839	41.150	42.222	43.903
XDLM($k=0.5$)	37.567	30.098	26.687	23.790	23.417	27.854	35.682	40.724	45.976	46.620
UDLM	43.316	34.525	30.381	28.086	26.242	23.619	31.188	35.963	38.588	41.801